

Damping Performance Enhancement of a Power System by STATCOM and its Frequency Stability Consideration

By

Mehedi Hassan

A thesis submitted in partial fulfillment of the requirements for the degree of
Master of Engineering
in Electrical & Electronic Engineering



Khulna University of Engineering & Technology
Khulna 9203, Bangladesh
December 2016

Declaration

This is to certify that the thesis work entitled "*Damping Performance Enhancement of a Power System by STATCOM and its Frequency Stability Consideration*" has been carried out by *Mehedi Hassan* in the Department of *Electrical and Electronic Engineering*, Khulna University of Engineering & Technology, Khulna, Bangladesh. The above thesis work or any part of this work has not been submitted anywhere for the award of any degree or diploma.

Signature of Supervisor

Signature of Candidate

Approval

This is to certify that the thesis work submitted by *Mehedi Hassan* entitled "*Damping Performance Enhancement of a Power System by STATCOM and its Frequency Stability Consideration*" has been approved by the board of examiners for the partial fulfillment of the requirements for the degree of *Master of Engineering* in the Department of *Electrical & Electronic Engineering*, Khulna University of Engineering & Technology, Khulna, Bangladesh in December, 2016.

BOARD OF EXAMINERS

- | | | |
|----|--|--------------------------|
| 1. | _____
Dr. Naruttam Kumar Roy
Assistant Professor
Department of Electrical & Electronic Engineering
Khulna University of Engineering & Technology | Chairman
(Supervisor) |
| 2. | _____
Head of the Department
Department of Electrical & Electronic Engineering
Khulna University of Engineering & Technology | Member |
| 3. | _____
Dr. Bashudeb Chandra Ghosh
Professor
Department of Electrical and Electronic Engineering
Khulna University of Engineering & Technology | Member |
| 4. | _____
Dr. Md. Abdur Rafiq
Professor
Department of Electrical and Electronic Engineering
Khulna University of Engineering & Technology | Member |
| 5. | _____
Dr. Md. Fayzur Rahman
Professor
Department of Electrical and Electronic Engineering
Green University of Bangladesh | Member
(External) |

ACKNOWLEDGEMENT

I would like to express my deepest gratitude to my supervisor and motivator **Dr. Naruttam Kumar Roy**, Assistant Professor, Department of Electrical & Electronic Engineering, Khulna University of Engineering & Technology, Khulna for his constant inspiration, valuable guidance and kind co-operation and finally helping me for providing necessary materials and sources during the entire period of my research work.

I am glad to thank all of my honorable teachers and supporting staffs in the department of Electrical & Electronic Engineering who have directly and indirectly helped me to do my job.

Last but not least, I would like to thank the authors of various research articles and books that are referred to.

ABSTRACT

This thesis investigates the damping performance of power systems through eigenvalue analysis and the impact of cyber-attack on power systems in frequency disturbing aspects during sudden changes of load. It also proposes a solution method to make the system stable. The analysis is firstly carried out on the Western System Coordinating Council (WSCC) 9-bus test system to find the impact of location of Flexible AC Transmission System (FACTS) devices on the static voltage stability. The maximum loadability of the load buses is determined using continuation power flow method with static var compensator (SVC) and static synchronous compensator (STATCOM). The result shows that the reactive power support from the FACTS devices depends on the proper placement of the FACTS devices in the network.

The analysis is then conducted on an IEEE 14-bus test system. The maximum loading limits of the load buses are determined using continuation power flow method and a static synchronous compensator (STATCOM) is installed as an objective to increase the systems loadability. Then, the dominant modes and associated states that affect the damping of the system are identified and an oscillation damping controller is designed. The result shows that the proposed damping controller equipped with STATCOM can improve the damping performance of the system significantly.

In order to analyze the impact of cyber attack on power systems, the stable limit of speed regulation for load frequency control (LFC) and integral controller gain for automatic generation control (AGC) is derived from their characteristic equations. Depending upon the nature of cyber-attack (positive biased or negative biased attack), simulations are performed to show the frequency deviations and oscillations of the power system. Finally, a feedback LFC block with a three input switch is proposed to remove these oscillations.

Contents

	PAGE
Title Page	i
Declaration	ii
Certificate of Research	iii
Acknowledgement	iv
Abstract	v
Contents	vi
List of Tables	ix
List of Figures	x
CHAPTER I	
Introduction	1
1.1 Research Background	1
1.1.1 Demand, Generation and Transmission of Electricity	1
1.1.2 Stability using FACTS	1
1.1.3 Cyber Threat on Modern Power Grid	3
1.2 Literature Review	4
1.2.1 Proper Placement of FACTS	4
1.2.2 Damping Controller with STATCOM	5
1.2.3 Smart-grid Cyber Vulnerability	5
1.3 Research Focuses	6
1.4 Thesis Outlines	6
CHAPTER II	
FACTS Device and Power Flow	8
2.1 Introduction	8
2.2 SVC	9
2.2.1 Introduction	9
2.2.2 Implemented SVC model	10
2.3 STATCOM	10
2.3.1. Introduction	10
2.3.2 Implemented STATCOM Model	11
2.4 Power Flow Analysis	12
2.4.1 Introduction	12
2.4.2 Formulation of the load flow problem	13
2.4.3 Newton-Raphson Approach	15
2.5 Continuation Power Flow	18
2.5.1 Introduction	18
2.5.2 Mathematical Reformulation	19
2.5.3 Prediction Step	20

	2.5.4 Correction Step	21
	2.6 Summary	22
CHAPTER III	LFC and AGC of Power System	23
	3.1 Introduction	23
	3.2 Load Frequency Control (LFC)	23
	3.2.1 Generator Model	23
	3.2.2 Load Model	24
	3.2.3 Prime Mover Model	25
	3.2.4 Governor Model	25
	3.2.5 Speed Regulation with LFC Loop	26
	3.3 Automatic Generation Control (AGC)	28
	3.3.1 Integral Controller with LFC	29
	3.4 Summary	30
CHAPTER IV	Enhancement of Damping Performance using STATCOM	31
	4.1 Introduction	31
	4.2 Voltage Stability Assessment	31
	4.2.1 System Model	31
	4.2.2 Static Voltage Stability Analysis	33
	4.3 Damping of Oscillation	37
	4.3.1 System Description	37
	4.3.2 Static and Dynamic Analysis	40
	4.3.3 Proposed Methodology	44
	4.4 Summary	46
CHAPTER V	Frequency Stability Improvement during Cyber-Attack	47
	5.1 Introduction	47
	5.2 Cyber-Attack Impact on LFC	47
	5.2.1 Result of Positively Biased Attack	49
	5.2.2 Result of Negatively Biased Attack	50
	5.3 Cyber-Attack Impact on AGC	50
	5.3.1 Positively Biased Attack	52
	5.3.2 Negatively Biased Attack	53
	5.4 Mitigation of Frequency Disturbance	55
	5.4.1 Effect of Sudden Load Change	55
	5.4.2 Proposed Solution	56
	5.5 Summary	58
CHAPTER VI	Conclusion and Future Work	59
	6.1 Contributions	59
	6.2 Future Work	60

References	61
Appendices	67
List of Publications	76

LIST OF TABLES

Table No	Description	Page
1.1	Noteworthy low frequency oscillation incidents in history	3
4.1	MLP with and without FACTS device	34
4.2	MLP and power loss for connection of STATCOM at different load buses	36
4.3	Critical mode of the considered system	42
5.1	Power system parameters	49
A.1	Data of WSCC 9-bus system	67
B.1	Line data of IEEE 14-bus test system	68
B.2	Load data of IEEE 14-bus test system	69

LIST OF FIGURES

Figure No	Description	Page
2.1	Static VAR Compensators (SVC): TCR/TSR, TSC, FC and Mechanically Switched Resistor	9
2.2	Block diagram of SVC	10
2.3	GTO-based STATCOM Simple Diagram	11
2.4	Block diagram of STATCOM	12
2.5	Single-line diagram of a simple example power system	13
2.6	Equivalent circuit for one phase of the system shown in Figure 2.5	13
2.7	Illustration of prediction-correction steps	19
2.8	Flow chart for continuation power flow	21
3.1	Block diagram of generator model	24
3.2	Generator and load model	24
3.3	Equivalent block diagram of generator-load model	25
3.4	The block diagram of a simple non-reheat steam turbine	25
3.5	Block diagram of speed governing system of a steam turbine	26
3.6	Load frequency control system	26
3.7	Frequency deviation step response for LFC (normal operating condition)	28
3.8	The AGC control system block diagram	29
3.9	Frequency deviation step response for AGC (normal operating condition)	30
4.1	WSCC 9-bus test system	31
4.2	Transmission line parameters	32
4.3	PV bus parameters	33
4.4	Bus voltages of the system	34
4.5	P-V curve without FACTS device	35
4.6	P-V curve with SVC installed at bus 8	35
4.7	P-V curve with STATCOM installed at bus 8	36

4.8	Bus voltages of the system with and without STATCOM (base case)	37
4.9	IEEE 14-bus test system	37
4.10	Model parameters of generator connected at bus 2	39
4.11	STATCOM with POD controller	40
4.12	Loading parameter-voltage curve under base case	40
4.13	Bus voltages of IEEE 14-bus test system under disturbance	43
4.14	Mechanical input power and electrical output power of synchronous generator 1	43
4.15	Implemented PSAT model of IEEE 14-bus test system with STATCOM and POD controller	45
4.16	Bus 1 Voltage	46
5.1	Equivalent block diagram of LFC	47
5.2	System Frequency deviation under different values of speed regulation	48
5.3	Frequency deviation in case of positively biased attack	49
5.4	Frequency deviation in case of negatively biased attack	50
5.5	The equivalent block diagram of AGC	51
5.6	Frequency deviation step response for different values of K_I	51
5.7	Frequency deviation due to positively biased attack	52
5.8	Frequency deviation due to negatively biased attack	53
5.9	Cyber attack impact on LFC and AGC at a glance	54
5.10	Frequency deviation step response (sudden load decrease)	55
5.11	Frequency deviation step response (sudden load increase)	55
5.12	Unstable frequency deviation (after cyber-attack)	56
5.13	LFC with a three input switch	57
5.14	Switch properties	57
5.15	Frequency deviation before and after using the switch during cyber-attack (sudden load increase and decrease)	58

CHAPTER I

Introduction

1.1 Research Background

1.1.1 Demand, Generation and Transmission of Electricity

Electricity can't be captured from moving air like wind energy or pumped out of the ground like oil. It is produced by the use of primary energy sources such as natural gas, coal, or nuclear reactions. So it is called a secondary source of energy. The demand of the electric power is greater today than ever before, with the rapid development of the social economy, science and technology. Shortage of the energy reserve has been widely recognized due to the excessive exploitation and utilization of these primary energy sources. Therefore, it is urgent to find a sustainable and effective way to address the energy problems in the long term.

During the last few years, renewable energy sources such as wind and solar energy seem to be better candidate for future electric power generation in terms of safety, cleanness and sustainability. The benefits of the renewable energies are now widely recognized and the utilization of renewable energies is now on a fast track. The amount of generating capacity added in wind and solar photovoltaic in 2015 came to 118GW, far above the next highest annual figure, 2014's 94GW [1].

The power transfer capability of the existing electric power transmission system is always finite and it will eventually move towards its working limits with the incremental power flow. The reinforcement of the existing transmission system cannot be simply achieved by adding new lines due to some economic, geographic and environmental issues. So, it is essential to find additional solutions to facilitate the upgrade and reinforcement of the existing transmission system with more flexibility and higher cost efficiency.

1.1.2 Stability using FACTS

Flexible AC transmission system, also known as FACTS, is not only able to provide a solution to the enhancement of power system transmission capability with great flexibility but also beneficial to improve power system stability.

Power system dynamic stability can be categorized as small-signal stability and transient stability [2]. Small-signal stability defines the ability of power systems to recover to its original steady state after small disturbances without losing synchronism. In normal power

system operations, small disturbances caused by random fluctuations in certain system parameters may excite power system oscillations; these oscillations are also known as low frequency oscillations since their frequencies (0.1Hz~2.0Hz) are relatively low comparing to the fundamental frequency of AC system (50/60Hz) [3].

Insufficient damping of low frequency oscillations is one of the main causes of small-signal instability; and even for a stable system, it is also important to make sure that the system has enough damping so that the settling time of the decaying oscillations can be minimized based on certain system operating requirements.

The following practices are normally suggested to increase system small-signal stability [2], in which, the first three approaches improve the small-signal stability of power systems inherently by reducing the electric distance between the synchronous generator and the grid; while PSS and FACTS supplementary damping controller could increase the power system damping against low frequency oscillations by the dynamic control of interrelated system parameters such as bus voltage and line power flow.

- Improve power system network topologies
- Increase real and reactive power reserve
- Improve the AVR (automatic voltage regulator) on excitation systems
- Install PSS (power system stabilizer) and FACTS supplementary damping controllers

Transient stability is the ability of power system to maintain synchronism subject to large disturbances such as system fault and transmission line outage. Different from small-signal stability, the transient stability of a particular system might be disparate with respect to different disturbances and the loss of synchronism caused by transient instability usually happens within 2 to 3 seconds after the disturbance, which is much faster than that caused by small-signal instability. To improve system transient stability, the following practices are suggested [2]:

- Fast fault clearance and auto-reclose
- Increase electromagnetic power output of the generator
- Decrease mechanical power output of the prime mover

Besides, reducing electric distance can also help enhancing transient stability in a certain degree.

Failing to address the dynamic stability issues may lead to serious consequences. Take low frequency oscillation for example, the loss of synchronism caused by low frequency oscillation can result in inter-connected system separation and even wide-area blackouts.

Some of the noteworthy low frequency oscillation incidents in history are summarized in Table 1-1 [4].

Table 1.1: Noteworthy low frequency oscillation incidents in history

Low frequency oscillation incident	Oscillation frequency
UK (1980)	0.50Hz
Taiwan (1984, 1989, 1990, 1991, 1992)	0.78-1.05Hz
West USA/Canada system separation (1996)	0.22Hz
Scandinavia (1997)	0.50Hz
China blackout (2003)	0.40Hz
USA blackout (2003)	0.17Hz
Italian blackout (2003)	0.55Hz

Based on different causes, low frequency oscillations can be classified as local oscillatory mode and inter-area oscillatory mode. The local oscillatory mode describes the oscillations between a single generator or a group of generators in the same area and the rest of the system with the frequency of 1.0 to 2.0Hz; while the inter-area oscillatory mode is aroused by generators or generator groups from different areas oscillating against each other with the frequency of 0.1 to 1.0Hz [3]. From Table 1-1, it should be noticed that these incidents are actually inter-area oscillations. In wide-area interconnected power systems, local oscillations can be effectively suppressed by the proper designs of AVR and PSS. However, for inter-area oscillations involving multiple areas, the regulations from the generator side could be quite limited. Therefore, it is essential to design FACTS supplementary damping controllers to mitigate the inter-area oscillations.

1.1.3 Cyber Threat on Modern Power Grid

Increased load on interconnected grid system is making the system heavily loaded day by day. Moreover, operational deregulation causes a dramatic change to modern electric power systems. All these make the power system vulnerable and less reliable. At the same time, the quality of power supply has become a critical issue due to the growth of electronic loads [5]. Considering all these aspects nowadays, there is a rising tendency of transition from a centralized power grid system to a local energy grid system with control capability called micro grid in case of an emergency and power shortage during power interruption in the main grid [6].

Micro grid can disconnect from the traditional grid and operate autonomously. Moreover, to enlighten remote areas, small scale power station is needed to set up where grid extension for power supply becomes costly and difficult. In many cases the availability of power supply

becomes the prime concern for medical treatment, technical research, industry, transportation etc. To ensure continuous power supply for all these cases, it is required to set up special generating station.

The renewable energy such as photovoltaic cells (PV), fuel cells, wind power etc. in combination with diesel generators are the main sources of power for these systems. A distributed and autonomous generation control is mandatory for these small power producing networks. They are generally connected to the grid at substation or customer loads. The power generated from PV, fuel cells are in the form of direct current whereas the power from wind generators, micro turbines are in the form of alternate current at a frequency different from the required 50 Hz. Therefore, a power electronic interface is required for the system containing these sources.

Since small scale islanded power systems can help in improving the power quality and power supply flexibility, it is also gaining attention to power utility companies. They can be used not only to provide spinning reserve but also to reduce the transmission and distribution costs. Also during the event of an outage in the primary substation they can be used to feed the customers.

Modern micro grid can supply power having the ability to change between islanded mode and grid-connected mode. It should ensure the reliability of the power supply that demands the necessity of controlling the power station smartly. To do so, advanced control system with communication interface should be adopted. For ensuring smooth power supply, stability of the system should be maintained properly.

In order to make the system stable its output parameter, especially voltage and frequency should be kept constant to its pre-assigned value. The whole system may collapse due to any disturbance of these output quantities. As being equipped with a smart control system, cyber threat on an islanded power station is considered to be a powerful means of disturbance that may cause the system severely unstable.

A detailed literature review in the area of power system voltage stability enhancement, damping control and cyber-attack impact is presented in the next section.

1.2 Literature Review

1.2.1 Proper Placement of FACTS

Power systems have become increasingly concerned world-wide with voltage stability and collapse problems [7]-[8]. A number of major voltage collapse phenomena have been experienced by utilities resulted in widespread blackouts [9]. In spite of dynamic nature of

voltage instability, static approaches are used for its analysis based on the fact that the system dynamics influencing voltage stability are usually slow [10]-[12].

Various theories have been established in voltage stability analysis through rigorous mathematical investigation [13]. A novel approach based on multi-input multi-output transfer function for analyzing static voltage stability is proposed in [14]. An improved neural network based algorithm is proposed to monitor voltage stability in [15]. Voltage sensitivity and modal analysis is used to investigate voltage stability in [16] which concludes that voltage stability margins have a precise voltage collapse point when a power system is subjected to sudden load increase. Voltage stability limit is usually dominant in heavily loaded systems [17]. As modern systems are being operated under heavily stressed conditions with reduced stability margins, incorporation of voltage stability analysis is essential for proper planning and control of power systems.

One of the main causes of voltage collapse is the inadequate reactive power in the system. Reactive power sources such as flexible AC transmission system (FACTS) devices can be used to improve the voltage stability of power systems [18]. However, as they are very expensive, they should not be placed without proper planning.

1.2.2 Damping Controller with STATCOM

In order to improve the stability of power systems, a static synchronous compensator (STATCOM) is increasingly popular [19], [20]. A STATCOM can dynamically support/absorb the reactive power to/from the power network and hence improves the system voltage profile and angle stability [21]. It can also enhance the overall stability of a power system if it is equipped with some more supplementary control signals.

The effect of different loads and voltage compensation using voltage source converter based STATCOM is presented in [22] which shows that, in some cases, it is hard to maintain the load angle close to unity. Time-domain analysis of a system with and without STATCOM is investigated in [23] for different types of faults in which inadequately damped oscillations are observed under certain critical conditions.

The disturbance in power system is mainly due to the connection/disconnection of large loads, faults, and loss of excitation in the generator [24]. The occurrence of contingencies in power system can cause poorly damped or even unstable oscillations which must be damped to ensure reliable power supply.

1.2.3 Smart-grid Cyber Vulnerability

Modern power system is largely dependent on information and communication technologies and digital computer techniques [25]. With the advancement of information and

communication technologies (ICT) and digital computer, advanced controllers are increasingly integrated into power generation and control system [26], [27]. These technologies greatly increase the dependency of the power system on ICT. This increasing dependency on ICT causes a harmful effect on power system through cyber-attack.

The cyber component of a power station is the advanced control loop, communication networking and sensors [28], [29]. The data for different parameters are collected using sensors and then these data are sent to controller [30], [31] for right operation of the system. The data sending action are performed using communication network which is one of the cyber vulnerable parts of the power system. The attacker can get the data when sending from sensing section to control section in a power station. After accessing the confidential data the attacker can get control on the automatic controller and change the controller action that results in malfunctioning of controller with changed set value. The malfunctioning leads to make the system unstable.

To ensure system stability cyber-attack impact on power system should be analyzed properly.

1.3 Research Focuses

Whenever a disturbance occurs in the system like generation/load imbalance or any fault caused by cyber-attack, the system may lose its stability or cause poorly damped oscillations. To improve the performance of system, the objectives of the research are as follows:

- Determining of the maximum loading point (MLP) of considered test power systems to analyze voltage stability.
- Determining the optimal place to install suitable FACTS devices for enhancing voltage stability and reducing power loss as the cost of these devices is very high.
- Determining the critical mode of power systems and associated participation factors through linear analysis.
- Evaluating the dynamic performance of power systems through nonlinear analysis.
- Designing a supplementary controller along with STATCOM for damping oscillations of power systems.
- Analyzing the frequency deviations and oscillations of an islanded power station during cyber-attack on its cyber vulnerable parts like load frequency Control (LFC) and automatic generation control (AGC).
- Determining the way of removing frequency deviations and oscillations significantly.

1.4 Thesis Outlines

This thesis is organized as follows:

Chapter II: FACTS Device and Power Flow

Chapter III: LFC and AGC of Power System

Chapter IV: Enhancement of Damping Performance using STATCOM

Chapter V: Frequency Stability Improvement during Cyber-Attack

Chapter VI: Conclusion and Future Work

CHAPTER II

FACTS Device and Power Flow

2.1 Introduction

Now a day as power demand increases the power system is getting more complex to fulfill the requirements within the acceptable quality and costs [32]. Generating stations are located away from the load centers because of economic and environmental issues. As the demand of power increases uncertainty occur in the system operation resulting reduction in stability and risk of blackouts. This problem can be tackle by introducing high power electronics controller in ac transmission networks. So “flexible” operation in ac transmission network comes in to role where changes can be done easily without affecting the systems. FACTS (Flexible Alternating Current Transmission System) are a family of power electronics device which improves stability, power transfer capability and controllability of ac system [33]. It also allows increasing the usable transmission capacity of its maximum thermal limits [34]

The IEEE Power Engineering Society (PES) Task Force of the FACTS Working Group has defined FACTS and FACTS Controller as given below [35].

Flexible AC Transmission System (FACTS): Alternating current transmission systems incorporating power electronic-based and other static controllers to enhance controllability and increase power transfer capability.

FACTS Controller: A power electronic-based system and other static equipment that provide control of one or more AC transmission system parameters.

Power flow through an ac line is a function of phase angle, line end voltages and line impedance, and there is little or no control over any of these variables. The consequences of this lack of fast, reliable control are stability problems, power flowing through other than the intended lines, the inability to fully utilize the transmission resources, undesirable var flows, higher losses, high or low voltages, cascade tripping and long restoration times.

With FACTS devices, power flow is electronically controlled and it flows as ordered by the control center [34]. Transmission capacity enhanced reasonably with using of appropriate type and rating of FACTS devices.

The range of FACTS devices include:

- Static Var Compensators (SVC)
- Static Compensators (STATCOM)
- Thyristor Controlled Series Capacitors (TCSC)
- Universal Power Flow Controllers (UPFC)
- High Voltage Direct Current Transmission (HVDC)

From these, this thesis will concentrate on the SVC and the STATCOM.

2.2 SVC

2.2.1 Introduction

The static var compensator regulates the voltage by controlling the amount of reactive power absorbed from or injected into the power system [36]. For example, it generates reactive power by switching capacitor banks when the system voltage is low or loads are inductive. Consequently, the reactive power demand of the lagging load is supplied by the SVC – relieving the distributing lines from delivering it. Thus, the voltage drop decreases and the voltage at the load terminals shall improve. Fig. 2.1 shows the configuration of a SVC. There are three common configurations of static var compensators which are given below.

1. Thyristor-controlled Reactors with Fixed Capacitors (TCR/FC)
2. Thyristor switched capacitors (TSC)
3. Thyristor-controlled Reactors and Thyristor switched Reactors (TCR/TSR)

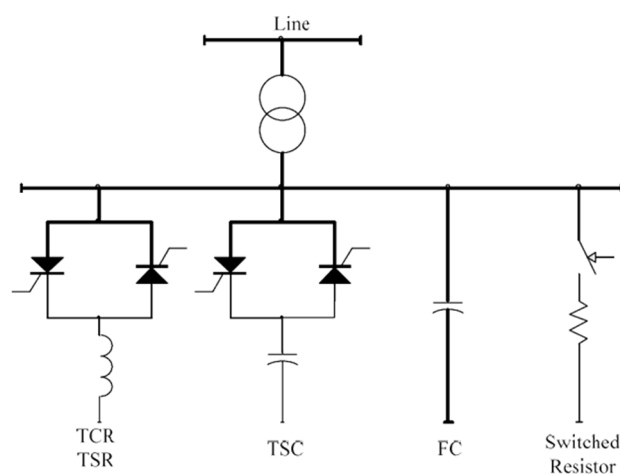


Figure 2.1: Static VAR Compensators (SVC): TCR/TSR, TSC, FC and Mechanically Switched Resistor

Likewise, the static var compensator absorbs reactive power when the system voltage is high or loads are capacitive. In this case, the SVC uses the reactors to consume the VARs from the system, thereby lowering the system voltage.

2.2.2 Implemented SVC model

In this thesis work, SVC model is used as a time constant regulator, as depicted in Fig. 2.2. In this model, a total reactance b_{SVC} is assumed and the following differential equation holds:

$$\dot{b}_{SVC} = (K_r(v_{ref} - v) - b_{SVC}) / T_r \quad (2.1)$$

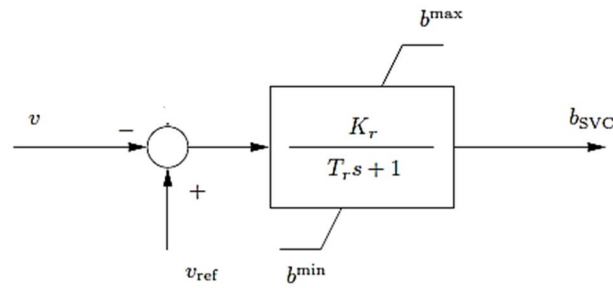


Figure 2.2: Block diagram of SVC [37].

Fig. 2.2 shows the block diagram of a SVC where v is the measured voltage at the connected bus, v_{ref} is the reference voltage, b^{max} and b^{min} is the maximum and minimum reactance, respectively, b_{SVC} is the total reactance, K_r is the regulator gain and T_r is the regulator time constant.

The model is completed by the algebraic equation expressing the reactive power injected at the SVC node:

$$q = b_{SVC}v^2 \quad (2.2)$$

The regulator has an anti-windup limiter, thus the reactance b_{SVC} is locked if one of its limits is reached and the first derivative is set to zero.

2.3 STATCOM

2.3.1. Introduction

STATCOM or Static Synchronous Compensator shown in Fig.2.3 is a shunt device, which uses force-commutated power electronics (i.e. GTO, IGBT) to control power flow and improve transient stability on electrical power networks [35].

A STATCOM has the following parts:

1. Voltage-Source Converter (VSC)
2. DC Capacitor
3. Inductive Reactance
4. Harmonic Filters

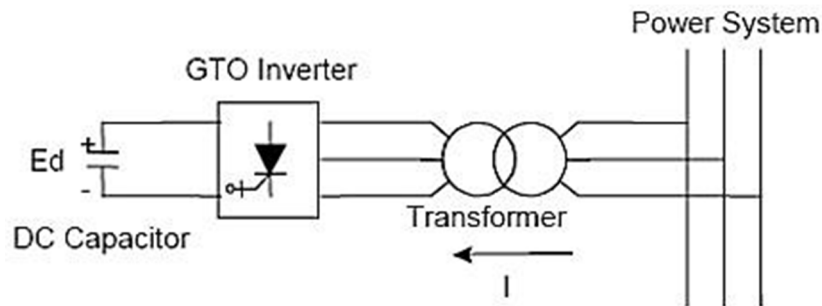


Figure 2.3: GTO-based STATCOM Simple Diagram [35]

In the case of two AC sources, which have the same frequency and are connected through a series reactance, the power flows will be [35]:

- Active or Real Power flows from the leading source to the lagging source.
- Reactive Power flows from the higher to the lower voltage magnitude source.

Consequently, the phase angle difference between the sources decides the active power flow, while the voltage magnitude difference between the sources determines the reactive power flow. Based on this principle, a STATCOM can be used to regulate the reactive power flow by changing the output voltage of the voltage-source converter with respect to the system voltage.

2.3.2 Implemented STATCOM Model

The implemented STATCOM model is a current injection model which is based on [38]-[40]. The STATCOM current is always kept in quadrature in relation to the bus voltage so that only reactive power is exchanged between the ac system and the STATCOM. The dynamic model is shown in Fig. 2.4, where it can be seen that the STATCOM assumes a time constant regulator like SVC.

The differential equation and the reactive power injected at the STATCOM node are given, respectively by:

$$i_{SH} = (K_r(v_{ref} - v) - i_{SH}) / T_r \quad (2.3)$$

$$q = i_{SH}V \quad (2.4)$$

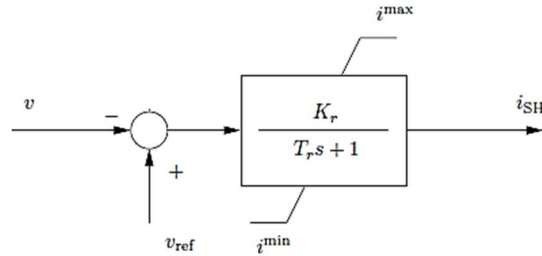


Figure 2.4: Block diagram of STATCOM [37].

Fig. 2.4 shows the block diagram of a STATCOM where v is the measured voltage at the connected bus, v_{ref} is the reference voltage, i^{max} and i^{min} is the maximum and minimum current, respectively, i_{SH} is the total injected current at the connected bus, K_r is the regulator gain and T_r is the regulator time constant.

The regulator has a non-windup limiter, thus the current i_{SH} is locked if one of its limits is reached and the first derivative is set to zero.

2.4 Power Flow Analysis

2.4.1 Introduction

Power flow or load flow study in power system is the steady state solution of the power system network. The power system is modeled by an electric network and solved for the steady-state powers and voltages at various buses. The direct analysis of the circuit is not possible, as the load are given in terms of complex powers rather than impedances, and generators behave more like power sources than voltage sources.

The main information obtained from the load flow study comprises of magnitudes and phase angles of load bus voltages, reactive powers and voltage phase angles at generator buses, real and reactive power flow on transmission lines together with power at the reference bus, other variables being specified. This information is essential for the continuous monitoring of the current state of the system and for the analyzing the effectiveness of the alternative plans for the future, such as adding new generator sites, meeting increased load demand and locating new transmission sites.

In load flow analysis, we are mainly interested in voltages at various buses and power injection into the transmission system. In addition, power flow analysis is required for many other analyses such as transient stability and contingency studies. The main objective of a power flow study is to determine the steady state operating condition of the electrical network. The steady state may be determined by finding out the flow of active and reactive power throughout the network and the voltage magnitudes and phase angles at all nodes of network. Such information is used to carry out security assessment analysis, where the nodal voltage magnitudes and active and reactive power flows in transmission lines and transformers are carefully observed to assess whether or not they are within prescribed operating limits. [41]-[43].

In solving a power flow problem, the system is assumed to be operating under balanced conditions and a single-phase model is used. In a power system each bus or node is associated with four quantities i.e. voltage magnitude $|V|$, phase angle δ , real power P , and reactive power Q . In a load flow solution two out of the four quantities are specified and the remaining two are required to be obtained through the solution of the equations. Based on the difference between power flow in the sending and receiving ends, the losses in a particular line can also be computed.

2.4.2 Formulation of the load flow problem

Load flow studies [44]-[45] are based on a nodal voltage analysis of a power system. As an example, a very simple system is considered that is represented by the single-line diagram in Fig. 2.5. Here two generators (1 and 2) are interconnected by one transmission line and are separately connected to a load (3) by two other lines. If the phasor currents injected into the system are I_1 , I_2 , and I_3 , and the lines are modeled by simple series admittances, then it is possible to draw the equivalent circuit for one representative phase of the balanced three-phase system, as shown in Fig. 2.6.

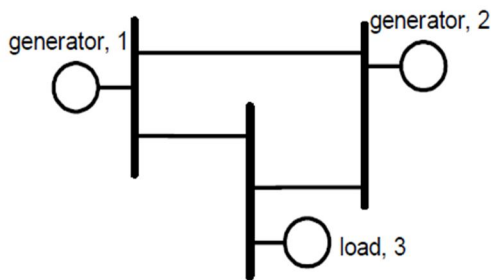


Figure 2.5: Single-line diagram of a simple example power system

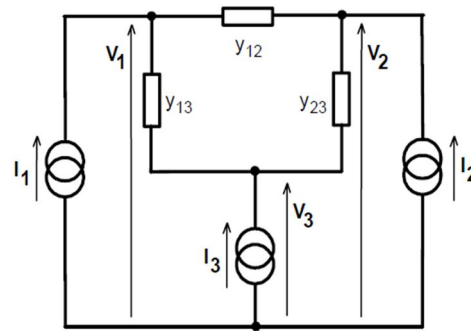


Figure 2.6: Equivalent circuit for one phase of the system shown in Figure 2.5

For the circuit in Fig. 2.6, the nodal voltage equations can be written directly. For example, at node 1:

$$\mathbf{I}_1 = (y_{12} + y_{13})\mathbf{V}_1 - y_{12}\mathbf{V}_2 - y_{13}\mathbf{V}_3 \quad (2.5)$$

In general, for a system with r nodes, then at node n :

$$\mathbf{I}_n = Y_{n1}\mathbf{V}_1 + Y_{n2}\mathbf{V}_2 + \dots + Y_{nn}\mathbf{V}_n + \dots + Y_{nr}\mathbf{V}_r = \sum_{k=1}^r Y_{nk}\mathbf{V}_k \quad (2.6)$$

where: Y_{nn} = sum of all admittances connected to node n

Y_{nk} = - (sum of all admittances connected between nodes n and k) = Y_{kn}

\mathbf{I}_n = current injected at node n

For the complete system of r nodes:

$$\begin{bmatrix} \mathbf{I}_1 \\ \vdots \\ \mathbf{I}_n \\ \vdots \\ \mathbf{I}_r \end{bmatrix} = \begin{bmatrix} Y_{11} & \dots & Y_{1n} & \dots & Y_{1r} \\ \vdots & & \vdots & & \vdots \\ Y_{n1} & \dots & Y_{nn} & \dots & Y_{nr} \\ \vdots & & \vdots & & \vdots \\ Y_{r1} & \dots & Y_{rn} & \dots & Y_{rr} \end{bmatrix} \begin{bmatrix} \mathbf{V}_1 \\ \vdots \\ \mathbf{V}_n \\ \vdots \\ \mathbf{V}_r \end{bmatrix} \quad \text{or} \quad [\mathbf{I}] = [\mathbf{Y}][\mathbf{V}] \quad (2.7)$$

Where, $[\mathbf{Y}]$ is the nodal admittance matrix. Formulation of the load flow problem is most conveniently carried out with the terms in the nodal admittance matrix expressed in polar notation: $Y_{kn} = Y_{kn} \angle \theta_{kn}$.

Conventional circuit analysis proceeds directly from equation (2.7) by inverting the nodal admittance matrix and hence solving for the nodal voltages $[\mathbf{V}]$. However, the load flow problem is complicated by the lack of uniformity in the data about electrical conditions at the nodes. There are three distinct types of nodal data, which relate to the physical nature of the power system:

a) Load nodes, where complex power $S_{ns} = P_{ns} + jQ_{ns}$ taken from or injected into the system is defined. Such nodes may also include links to other systems. At these load nodes, the voltage magnitude $|V_n|$ and phase angle δ_n must be calculated.

b) Generator nodes, where the injected power, P_{ns} , and the magnitude of the nodal voltage $|V_n|$ are specified. These constraints reflect the generator's operating characteristics, in which power is controlled by the governor and terminal voltage is controlled by the automatic voltage regulator. At the generator nodes the voltage phase angle δ_n must be calculated.

c) At least one node, termed the ‘floating bus’ or ‘slack bus’, where the nodal voltage magnitude $|V_n|$ and phase angle δ_n are specified. This node acts as the reference node and is commonly chosen to have a phase angle $\delta_n = 0^\circ$. The power and reactive power delivered at this node are not specified.

In the system configuration of Fig. 2.5, each type of node is represented with node 1 being a floating bus, node 2 being a generator node and node 3 being a load node. Consequently values must be specified for the power (P_{2s}) injected at node 2, and the power (P_{3s}) and reactive power (Q_{3s}) injected at node 3. All three of these power values may be changed by the user, though default values are provided ($P_{2s} = 1.0$; $P_{3s} = -1.5$; $Q_{3s} = -0.2$), with negative values indicating that power or reactive power is being drawn from the system.

The magnitude of the voltage at node 1 can be specified, with the default value being 1.0 pu, while the phase angle is fixed at 0° ($= 1.0 \angle 0^\circ V_1$). At the generator node (node 2), the voltage magnitude can be set by the user with the default value being 1.1 pu ($V_2 = 1.1 \angle \delta_2$), and the phase angle δ_2 is calculated during the load flow solution. At the load node (node 3) the voltage magnitude and phase have to be calculated ($V_3 = |V| \angle \delta_3$). So the complete load flow problem for this particular power system configuration involves the calculation of the voltage magnitude V_3 and the phase angles δ_2, δ_3 .

2.4.3 Newton-Raphson Approach

The Newton-Raphson (NR) method [46] is a powerful method of solving non-linear algebraic equations. Because of its quadratic convergence, Newton’s method is mathematically superior to the Gauss-Seidel method and is less prone to divergence with ill-conditioned problems. It works faster, and is sure to converge in most cases as compared to the Gauss-Siedel (GS) method.

It is indeed the practical method of load flow solution of large power networks. Its only drawback is the large requirement of computer memory, which can be overcome through a compact storage scheme. One of the main strengths of the Newton-Raphson method is its reliability towards convergence. Contrary to non Newton-Raphson solutions, convergence is independent of the size of the network being solved and the number and kinds of control equipment present in the system. Hence in the proposed work Newton-Raphson method is preferred.

The Newton-Raphson method is an iterative technique for solving systems of simultaneous equations in the general form:

$$\begin{aligned}
f_1(X_1, \dots, X_n, \dots, X_r) &= k_1 \\
f_n(X_1, \dots, X_n, \dots, X_r) &= k_n \\
f_r(X_1, \dots, X_n, \dots, X_r) &= k_r
\end{aligned} \tag{2.8}$$

where $f_1, \dots, f_n, \dots, f_r$ are differentiable functions of the variables $X_1, \dots, X_n, \dots, X_r$ and $k_1, \dots, k_n, \dots, k_r$ are constants. Applied to the load flow problem, the variables are the nodal voltage magnitudes and phase angles, the functions are the relationships between power, reactive power and node voltages, while the constants are the specified values of power and reactive power at the generator and load nodes. Power and reactive power functions can be derived by starting from the general expression for injected current (Eqn. 2.6) at node n:

$$I_n = \sum_{k=1}^r Y_{nk} V_k$$

so the complex power input to the system at node n is:

$$S_n = V_n I_n^* \tag{2.9}$$

where the superscript * denotes the complex conjugate. Substituting from (2.6) with all complex variables written in polar form:

$$S_n = V_n \sum_{k=1}^r Y_{nk}^* V_k^* = \sum_{k=1}^r |V_n| |V_k| |Y_{nk}| \angle \{\delta_n - \delta_k - \theta_{nk}\} \tag{2.10}$$

The power and reactive power inputs at node n are derived by taking the real and imaginary parts of the complex power:

$$P_n = \Re\{S_n\} = \sum_{k=1}^r |V_n| |V_k| |Y_{nk}| \cos\{\delta_n - \delta_k - \theta_{nk}\} \tag{2.11}$$

$$Q_n = \Im\{S_n\} = \sum_{k=1}^r |V_n| |V_k| |Y_{nk}| \sin\{\delta_n - \delta_k - \theta_{nk}\} \tag{2.12}$$

The load flow problem is to find values of voltage magnitude and phase angle, which, when substituted into (2.11) and (2.12), produce values of power and reactive power equal to the specified set values at that node, P_{ns} and Q_{ns} .

The first step in the solution is to make initial estimates of all the variables: $|V_n^0|, \delta_n^0$ where the superscript ⁰ indicates the number of iterative cycles completed. Using these estimates, the power and reactive power input at each node can be calculated from (2.11) and (2.12). These

values are compared with the specified values to give a power and reactive power error. For node n:

$$\Delta P_n^0 = P_{ns} - \sum_{k=1}^r |V_n^0| |V_k^0| |Y_{nk}| \cos\{\delta_n^0 - \delta_k^0 - \theta_{nk}\} \quad (2.13)$$

$$\Delta Q_n^0 = Q_{ns} - \sum_{k=1}^r |V_n^0| |V_k^0| |Y_{nk}| \sin\{\delta_n^0 - \delta_k^0 - \theta_{nk}\} \quad (2.14)$$

The power and reactive power errors at each node are related to the errors in the voltage magnitudes and phase angles, e.g. $\Delta|V_n^0|, \Delta\delta_n^0$ by the first order approximations:

$$\begin{bmatrix} \vdots \\ \Delta P_n^0 \\ \vdots \\ \vdots \\ \Delta Q_n^0 \\ \vdots \end{bmatrix} = \begin{bmatrix} \vdots & \vdots & \vdots & \vdots & \vdots & \vdots & \vdots & \vdots & \vdots & \vdots \\ \vdots & \frac{\partial P_n}{\partial \delta_{n-1}} & \frac{\partial P_n}{\partial \delta_n} & \frac{\partial P_n}{\partial \delta_{n+1}} & \vdots & \vdots & \vdots & \frac{\partial P_n}{\partial |V_{n-1}|} & \frac{\partial P_n}{\partial |V_n|} & \frac{\partial P_n}{\partial |V_{n+1}|} \\ \vdots & \vdots & \vdots & \vdots & \vdots & \vdots & \vdots & \vdots & \vdots & \vdots \\ \vdots & \vdots & \vdots & \vdots & \vdots & \vdots & \vdots & \vdots & \vdots & \vdots \\ \vdots & \vdots & \vdots & \vdots & \vdots & \vdots & \vdots & \vdots & \vdots & \vdots \\ \vdots & \frac{\partial Q_n}{\partial \delta_{n-1}} & \frac{\partial Q_n}{\partial \delta_n} & \frac{\partial Q_n}{\partial \delta_{n+1}} & \vdots & \vdots & \vdots & \frac{\partial Q_n}{\partial |V_{n-1}|} & \frac{\partial Q_n}{\partial |V_n|} & \frac{\partial Q_n}{\partial |V_{n+1}|} \\ \vdots & \vdots & \vdots & \vdots & \vdots & \vdots & \vdots & \vdots & \vdots & \vdots \end{bmatrix} \begin{bmatrix} \Delta\delta_{n-1}^0 \\ \Delta\delta_n^0 \\ \Delta\delta_{n+1}^0 \\ \vdots \\ \Delta|V_{n-1}|^0 \\ \Delta|V_n|^0 \\ \Delta|V_{n+1}|^0 \end{bmatrix} \quad (2.15)$$

where the matrix of partial differentials is called the Jacobian matrix, [J]. The elements of the Jacobian are calculated by differentiating the power and reactive power expressions (2.11), (2.12) and substituting the estimated values of voltage magnitude and phase angle. At the next stage of the Newton-Raphson solution, the Jacobian is inverted. Matrix inversion is a computationally-complex task with the resources of time and storage increasing rapidly with the order of [J]. This requirement for matrix inversion is a major drawback of the Newton-Raphson method of load flow analysis for large-scale power systems. However, with the inversion completed, the approximate errors in voltage magnitudes and phase angles can be calculated by pre-multiplying both sides of (2.15):

$$\begin{bmatrix} \Delta\delta_{n-1}^0 \\ \Delta\delta_n^0 \\ \Delta\delta_{n+1}^0 \\ \vdots \\ \Delta|V_{n-1}|^0 \\ \Delta|V_n|^0 \\ \Delta|V_{n+1}|^0 \end{bmatrix} = \begin{bmatrix} J^0 \end{bmatrix}^{-1} \begin{bmatrix} \vdots \\ \Delta P_n^0 \\ \vdots \\ \vdots \\ \Delta Q_n^0 \\ \vdots \end{bmatrix} \quad (2.16)$$

The approximate errors from (2.16) are added to the initial estimates to produce new estimated values of node voltage magnitude and angle. For node n :

$$|V_n^1| = |V_n^0| + \Delta|V_n^0| \quad (2.17)$$

$$\delta_n^1 = \delta_n^0 + \Delta\delta_n^0 \quad (2.18)$$

Because first-order approximations are used in (2.15) the new estimates (denoted by the superscript 1) are not exact solutions to the problem. However, they can be used in another iterative cycle, involving the solution of Equations (2.13-2.18). The process is repeated until the differences between successive estimates are within an acceptable tolerance band.

The description above relates specifically to a load node, where there are two unknowns (the voltage magnitude and angle) and two equations relating to the specified power and reactive power. For a generator node the voltage magnitude $|V_n|$ and power P_n are specified, but the reactive power is not specified. The order of the calculation can be reduced by 1. There is no need to ensure that the reactive power is at a set value and only the angle of the node voltage needs to be calculated, so one row and column are removed from the Jacobian. For the floating bus, both voltage magnitude and angle are specified, so there is no need to calculate these quantities.

2.5 Continuation Power Flow

2.5.1 Introduction

The Jacobian matrix of power flow equations becomes singular at the voltage stability limit. Continuation power flow overcomes this problem. Continuation power flow finds successive load flow solutions according to a load scenario. It consists of prediction and correction steps. From a known base solution, a tangent predictor is used so as to estimate next solution for a specified pattern of load increase. The corrector step then determines the exact solution using Newton-Raphson technique employed by a conventional power flow. After that a new prediction is made for a specified increase in load based upon the new tangent vector. Then corrector step is applied. This process goes until critical point is reached. The critical point is the point where the tangent vector is zero. The illustration of predictor-corrector scheme is depicted in Fig. 2.7.

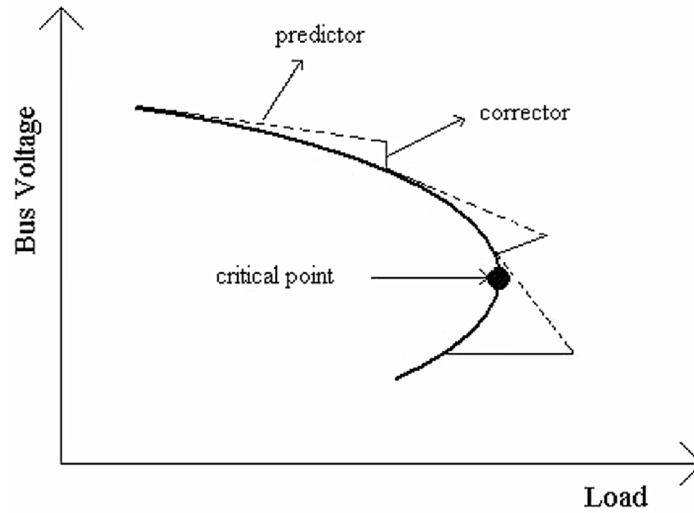


Figure 2.7: Illustration of prediction-correction steps

In continuation load flow, first power flow equations are reformulated by inserting a load parameter into these equations [47].

2.5.2 Mathematical Reformulation

Injected powers can be written for the i^{th} bus of an n -bus system as follows [48]:

$$P_i = \sum_{k=1}^n |V_i||V_k| (G_{ik}\cos\theta_{ik} + B_{ik}\sin\theta_{ik})$$

$$Q_i = \sum_{k=1}^n |V_i||V_k| (G_{ik}\sin\theta_{ik} + B_{ik}\cos\theta_{ik}) \quad (2.19)$$

$$P_i = P_{Gi} - P_{Di}, Q_i = Q_{Gi} - Q_{Di} \quad (2.20)$$

where the subscripts G and D denote generation and load demand respectively on the related bus.

In order to simulate a load change, a load parameter λ is inserted into demand powers P_{Di} and Q_{Di} .

$$P_{Di} = P_{Dio} - \lambda(P_{\Delta base})$$

$$Q_{Di} = Q_{Dio} - \lambda(Q_{\Delta base}) \quad (2.21)$$

P_{Dio} and Q_{Dio} are original load demands on i^{th} bus whereas $P_{\Delta base}$ and $Q_{\Delta base}$ are given quantities of powers chosen to scale λ appropriately. After substituting new demand powers in Equation (2.21) to Equation (2.20), new set of equations can be represented as:

$$F(\theta, V, \lambda) = 0 \quad (2.22)$$

where θ denotes the vector of bus voltage angles and V denotes the vector of bus voltage magnitudes. The base solution for $\lambda = 0$ is found via a power flow. Then, the continuation and parameterization processes are applied [49], [50].

2.5.3 Prediction Step

In this step, a linear approximation is used by taking an appropriately sized step in a direction tangent to the solution path. Therefore, the derivative of both sides of Equation (2.22) is taken.

$$F_{\theta}d\theta + F_VdV + F_{\lambda}d\lambda = 0$$

$$[F_{\theta} \ F_V \ F_{\lambda}] \begin{bmatrix} d\theta \\ dV \\ d\lambda \end{bmatrix} = \underline{0} \quad (2.23)$$

In order to solve Equation (2.23), one more equation is needed since an unknown variable λ is added to load flow equations. This can be satisfied by setting one of the tangent vector components to +1 or -1 which is also called continuation parameter. Setting one of the tangent vector components +1 or -1 imposes a non-zero value on the tangent vector and makes Jacobian nonsingular at the critical point. As a result Equation (2.23) becomes:

$$\begin{bmatrix} F_{\theta} & F_V & F_{\lambda} \\ \underline{e}_k & & \end{bmatrix} \begin{bmatrix} d\theta \\ dV \\ d\lambda \end{bmatrix} = \begin{bmatrix} 0 \\ \pm 1 \end{bmatrix} \quad (2.24)$$

where e_k is the appropriate row vector with all elements equal to zero except the k^{th} element equals 1. At first step λ is chosen as the continuation parameter. As the process continues, the state variable with the greatest rate of change is selected as continuation parameter due to nature of parameterization. By solving Equation (2.24), the tangent vector can be found. Then, the prediction can be made as follows:

$$\begin{bmatrix} \theta \\ V \\ \lambda \end{bmatrix}^{p+1} = \begin{bmatrix} \theta \\ V \\ \lambda \end{bmatrix}^p + \sigma \begin{bmatrix} d\theta \\ dV \\ d\lambda \end{bmatrix} \quad (2.25)$$

where the subscript “p+1” denotes the next predicted solution. The step size σ is chosen so that the predicted solution is within the radius of convergence of the corrector. If it is not satisfied, a smaller step size is chosen.

2.5.4 Correction Step

In correction step, the predicted solution is corrected by using local parameterization. The original set of equation is increased by one equation that specifies the value of state variable chosen and it results in:

$$\begin{bmatrix} F(\theta, V, \lambda) \\ x_k - \eta \end{bmatrix} = [0] \quad (2.26)$$

where x_k is the state variable chosen as continuation parameter and η is the predicted value of this state variable. Equation (2.26) can be solved by using a slightly modified Newton-Raphson power flow method.

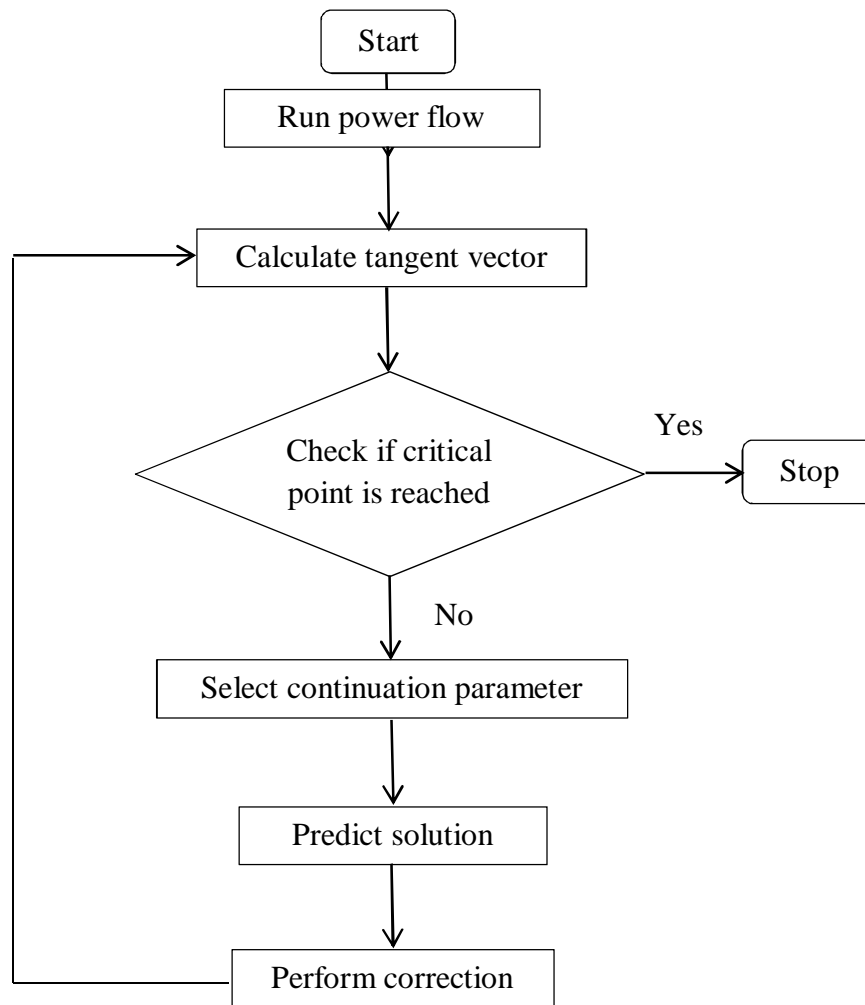


Figure 2.8: Flow chart for continuation power flow [47]

2.6 Summary

This chapter introduces two commonly used shunt connected FACTS devices; SVC and STATCOM, their implemented model and the process of Newton-Raphson power flow for controlling specific system parameters such as line power flow and bus voltages. Hence, the modeling of these FACTS includes the internal dynamics of FACTS devices as well as provides voltage support when installed on heavily loaded areas of power system.

CHAPTER 3

LFC and AGC of Power System

3.1 Introduction

To analyze the impact of cyber-attack on LFC and AGC system, it is important to know the operation of the control systems and their design models clearly. The primary objectives of LFC are to maintain the system frequency in stable, to divide the load between generators, and to control the tie-line interchange schedules. In an interconnected system consisting of several pools, the role of the AGC is to divide the loads among system, stations, and generators so as to achieve maximum economy and correctly control the scheduled interchanges of tie-line power while maintaining a reasonably uniform frequency.

3.2 Load Frequency Control (LFC)

In LFC system, the change in frequency and tie-line real power are sensed, which are a measure of the change in rotor angle δ . The error signals (Δf and ΔP_{tie}) are amplified, mixed, and transformed into a real power command signal ΔP_V , which is sent to the prime mover to call for an increment in the torque. The prime mover, therefore, brings change in the generator output by an amount ΔP_g which will change the values of Δf and ΔP_{tie} within the specified tolerance. In order to design and analysis of a control system, knowing of the mathematical modeling of the system is essential. In the following sections modeling of different systems are described.

3.2.1 Generator Model

The swing equation [51] of a synchronous machine is

$$\frac{2H}{\omega_s} \frac{d^2 \Delta \delta}{dt^2} = \Delta P_m - \Delta P_e \quad (3.1)$$

In terms of small deviation in speed, the above equation can be written as the following.

$$\frac{d \Delta \frac{\omega}{\omega_s}}{dt} = \frac{1}{2H} (\Delta P_m - \Delta P_e) \quad (3.2)$$

With speed in per unit expression the equation (3.2) transforms as

$$\frac{d\Delta\omega}{dt} = \frac{1}{2H}(\Delta P_m - \Delta P_e) \quad (3.3)$$

Taking the Laplace transform of equation (3.3)

$$\Delta\Omega(s) = \frac{1}{2Hs}[\Delta P_m(s) - \Delta P_e(s)] \quad (3.4)$$

The equation (3.4) can be expressed in terms of block diagram [52] shown in Fig. 3.1.

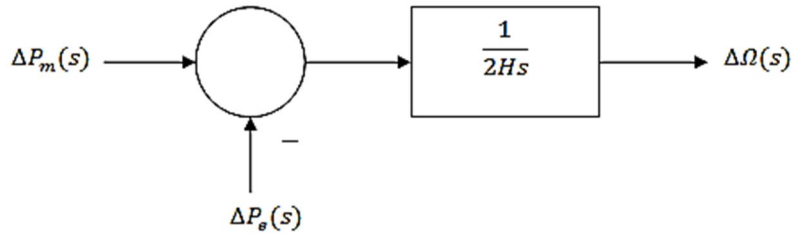


Figure 3.1: Block diagram of generator model.

3.2.2 Load Model

Power system contains varieties of loads. The resistive loads such as lighting and heating loads are independent of frequency. Motor loads are sensitive to changes in frequency. The sensitivity to frequency depends on the composite of the speed-load characteristics of all the driven devices. The speed-load characteristic of a composite load is expressed as

$$\Delta P_e = \Delta P_L + D\Delta\omega \quad (3.5)$$

Where ΔP_L is the non-frequency-sensitive load change and $D\Delta\omega$ is the frequency-sensitive load change. D is the percentage change in load divided by percentage change in frequency. Including this load model in the generator model, the combined block diagram [52] comes to the following one.

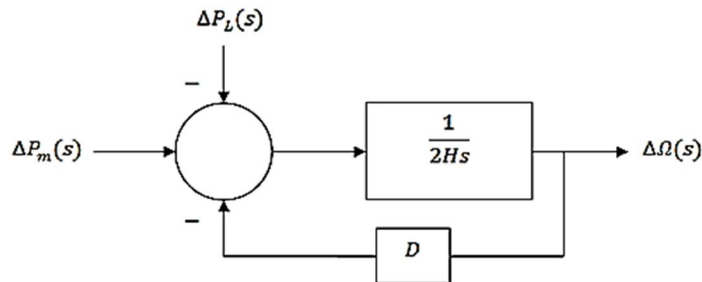


Figure 3.2: Generator and load model.

Eliminating the simple feedback loop from Fig. 3.2 generator-load model can be expressed as

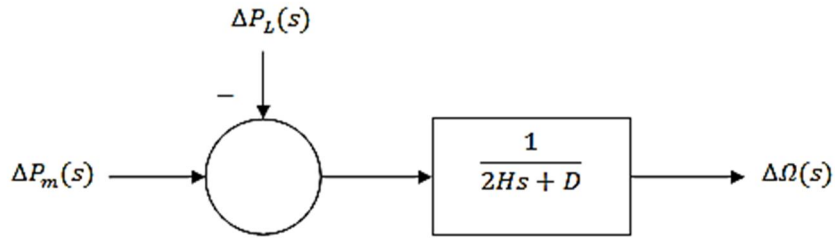


Figure 3.3: Equivalent block diagram of generator-load model.

3.2.3 Prime Mover Model

The source of mechanical power, usually known as the prime mover, may be hydraulic turbines at waterfalls, steam turbines whose energy comes from the burning of coal, gas, nuclear fuel, and gas turbines. The model for the turbine relates changes in mechanical power output ΔP_m to changes in steam valve position ΔP_v . The simplest prime mover model for non-reheat steam turbine with a single time constant τ_T , has the following transfer function.

$$G_T(s) = \frac{\Delta P_m(s)}{\Delta P_v(s)} = \frac{1}{1 + \tau_T(s)} \quad (3.6)$$

The block diagram of the above transfer function is

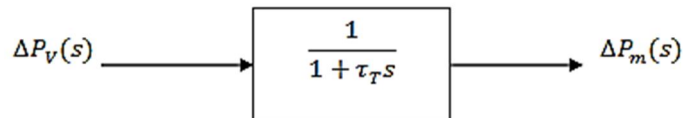


Figure 3.4: The block diagram of a simple non-reheat steam turbine.

3.2.4 Governor Model

When the generator electrical load is suddenly increased, the electrical power exceeds the mechanical power input. This power deficiency is supplied by the kinetic energy stored in the rotating system. The reduction in kinetic energy causes the turbine speed and, consequently, the generator frequency to fall. The change in speed is sensed by the turbine governor which acts to adjust the turbine input valve to change the mechanical power output to bring the speed to a new steady-state. For stable operation, the governors are designed to permit the speed to drop as the load increased. Let the slope of the speed reduction curve of the governor is R which is also regarded as the speed regulation. The speed governor mechanism acts as a comparator whose output ΔP_g is the difference between reference set power ΔP_{ref} and the power $(1/R) \Delta \omega$ i.e.

$$\Delta P_g = \Delta P_{ref} - \frac{1}{R} \Delta \omega \quad (3.7)$$

In s domain the equation can be written as the following

$$\Delta P_g(s) = \Delta P_{ref}(s) - \frac{1}{R} \Delta \Omega(s) \quad (3.8)$$

The command ΔP_g is transformed through the hydraulic amplifier to the steam valve position command ΔP_v . Assuming a linear relationship and considering a simple time constant τ_g , s domain relation can be expressed as

$$\Delta P_v(s) = \frac{1}{1 + \tau_g s} \Delta P_g(s) \quad (3.9)$$

Finally the governor model [52] can be written as the following block diagram.

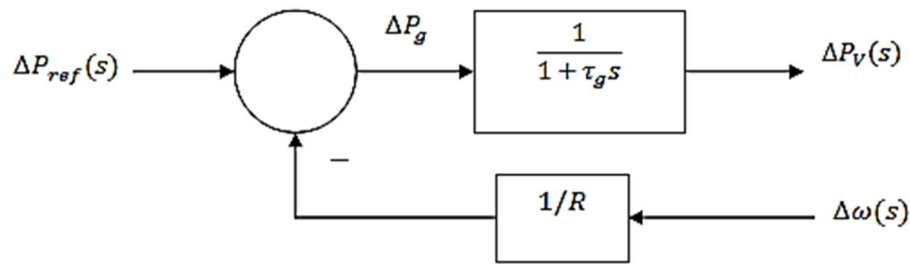


Figure 3.5: Block diagram of speed governing system of a steam turbine.

3.2.5 Speed Regulation with LFC Loop

Combining various models shown in the above sections finally the load frequency control loop [52] comes to the diagram shown in Fig. 3.6.

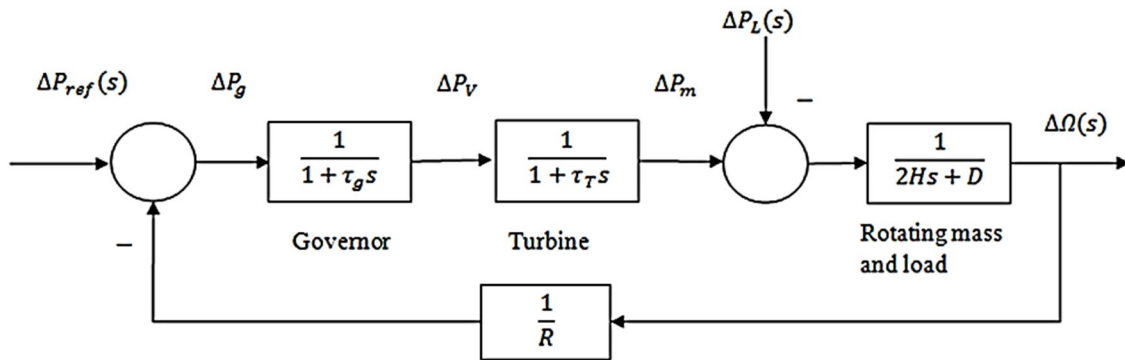


Figure 3.6: Load frequency control system.

For stable operation of LFC, determination of the stable limit of R is so important and it can be done using Routh-Hurwitz array. Before obtaining the stable limit of R, characteristic equation of the control system is required to determine.

The characteristic equation of the LFC loop is

$$1 + \frac{1}{R(2Hs + D)(1 + \tau_g s)(1 + \tau_T s)} = 0 \quad (3.10)$$

Considering $K=1/R$, the above equation becomes

$$1 + \frac{K}{(2Hs + D)(1 + \tau_g s)(1 + \tau_T s)} = 0 \quad (3.11)$$

Assuming an islanded power station has the following parameters.

Turbine time constant $\tau_T = 0.5$ sec

Governor time constant $\tau_g = 0.2$ sec

Governor inertia constant $H = 5$ sec

The variation of load with 1 percent change in frequency $D = 0.8$

Putting these assumed values into equation (3.11).

$$1 + \frac{K}{(10s + 0.8)(1 + 0.2s)(1 + 0.5s)} = 0$$

$$\text{or, } 1 + \frac{K}{(s^3 + 7.08s^2 + 10.56s + 0.8)} = 0$$

$$\text{or, } s^3 + 7.08s^2 + 10.56s + 0.8 + K = 0$$

The Routh-Hurwitz array for this polynomial is

s^3	1	10.56
s^2	7.08	0.8+K
s^1	$(73.965-K)/7.08$	0
s^0	0.8+K	0

From s^1 row it is seen that for system stability K must be less than 73.965 and from s^0 row K must be greater than -0.8.

Since $K = 1/R$, for control system stability R must be $R > 1/73.965$ or $R > 0.0135$.

The auxiliary equation from the s^2 row is $7.08s^2 + 74.765 = 0$ (For $K = 73.965$)

Or, $s = \pm j3.25$

For $R = 0.0135$ the system has conjugate poles on the $j\omega$ axis and the system will be marginally stable. So for stable operation of the system the value of R must be greater than 0.0135.

Using MATLAB, the performance curve of LFC block is shown in Fig. 3.7.

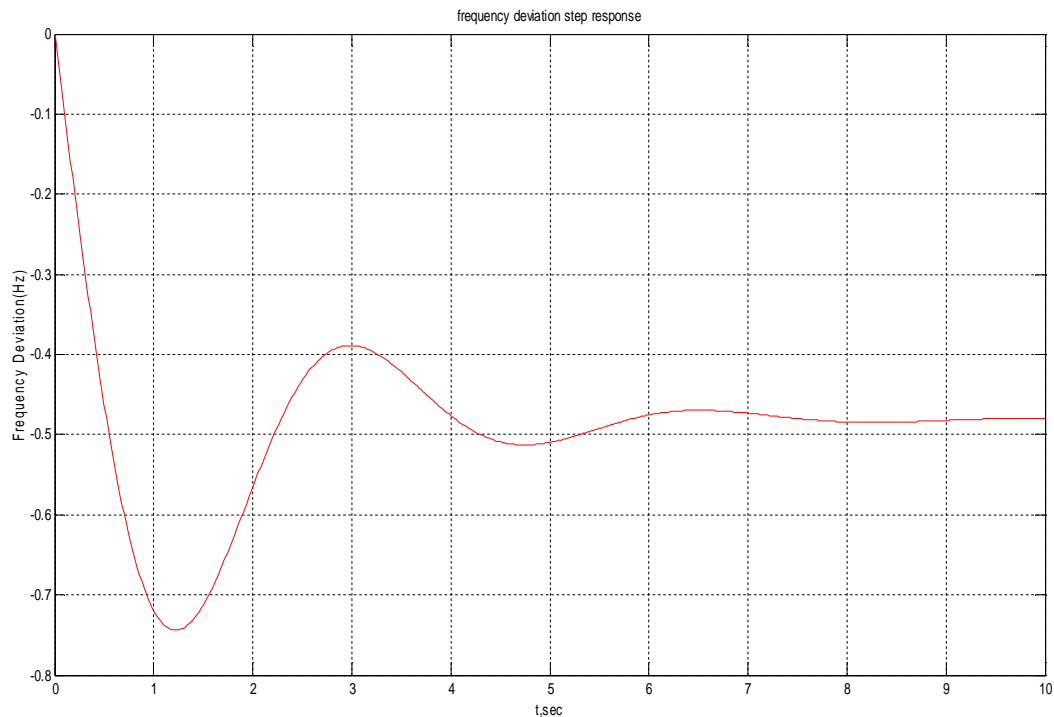


Figure 3.7: Frequency deviation step response for LFC (normal operating condition)

3.3 Automatic Generation Control (AGC)

When the load of the system is increased, the governor cannot adjust the input of the steam to the new load immediately whereas the turbine speed drops. The error signal becomes smaller with the reduction of the change of speed and the position of the governor fly-balls gets closer to the point required to maintain a constant speed. However, the constant speed will not be the set point, and there will be an offset. An integrator can solve the problem by restoring the speed or frequency to its nominal value.

The integral unit monitors the average error over a period of time and will overcome the offset. Thus, as the system load changes continuously, the generation is adjusted automatically to restore the frequency to the nominal value. This scheme is known as the Automatic Generation Control (AGC). AGC is nothing but LFC with parallel combination of integral controller. In Fig. 3.8, various functional parts of AGC are shown.

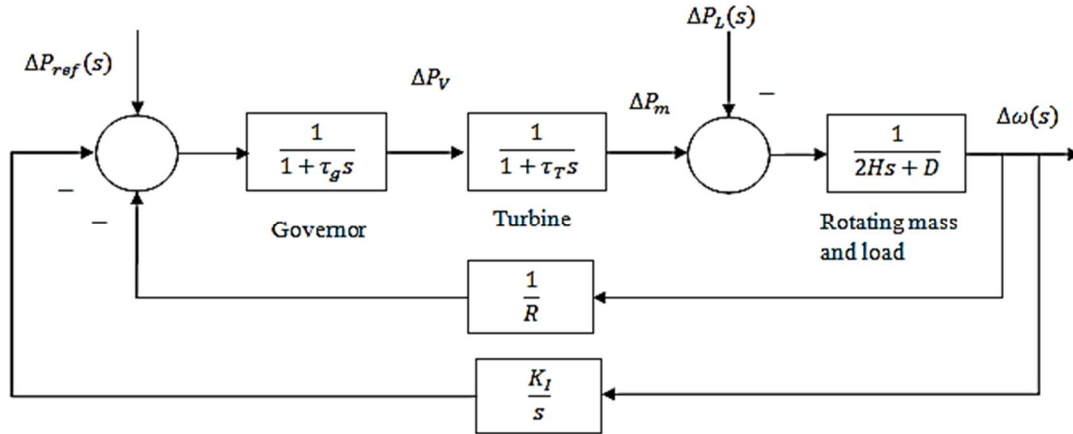


Figure 3.8: The AGC control system block diagram [52].

3.3.1 Integral Controller with LFC

With the primary LFC loop, a change in the system load will result in a steady-state frequency deviation, depending on the governor speed regulation. In order to reduce the frequency deviation to zero, a rest action must be provided. The rest action can be achieved by introducing an integral controller to act on the load reference setting to change the speed set point. The controller increases the system type by 1 which forces the final frequency deviation to zero. The integral controller gain K_I must be adjusted for a satisfactory transient response.

The difference between primary LFC loop and AGC can be easily determined from their performance curves. To draw the performance curves same assumptions that were considered in LFC loop are used in Fig. 3.9 also.

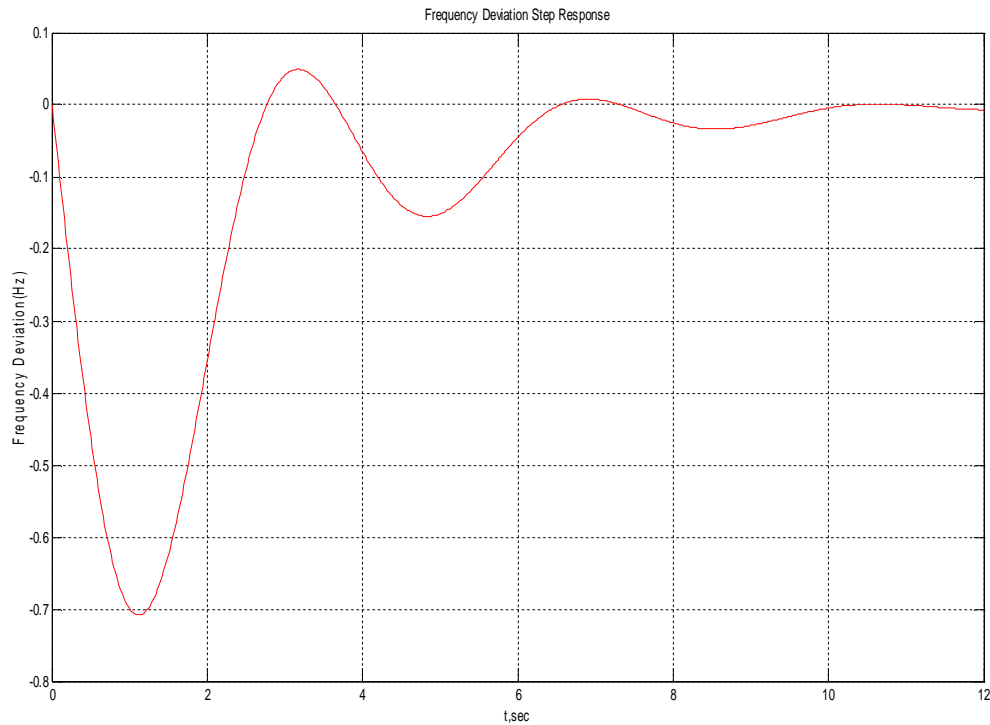


Figure 3.9: Frequency deviation step response for AGC (normal operating condition)

3.4 Summary

This chapter discusses the mathematical modeling and performance curves of LFC and AGC with their block diagram in detail. From their performance curves, it is noticeable that the use of integral controller with primary LFC loop, the frequency deviation can be reduced to zero with proper selection of integral controller gain K_I .

CHAPTER IV

Enhancement of Damping Performance using STATCOM

4.1 Introduction

The continued growth in demand for electric power can be met by increased loading of available power lines that leads to a poorly damped power oscillations between generators. With the evolution of power electronics, flexible AC transmission systems (FACTS) controllers have created the scope to improve power oscillations damping by controlling the power flow over the AC transmission line.

4.2 Voltage Stability Assessment

4.2.1 System Model

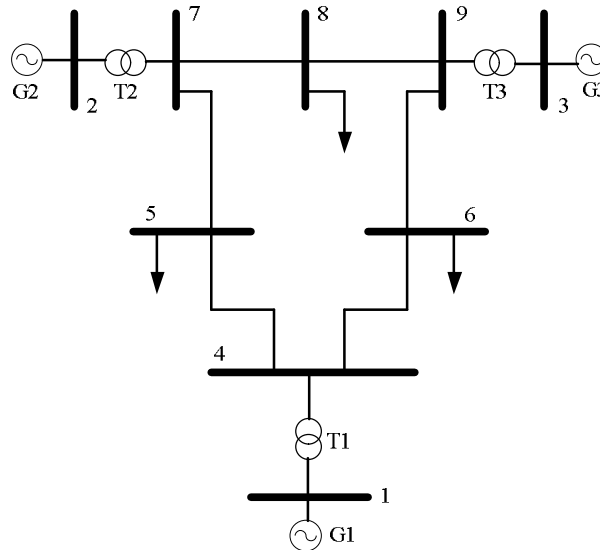
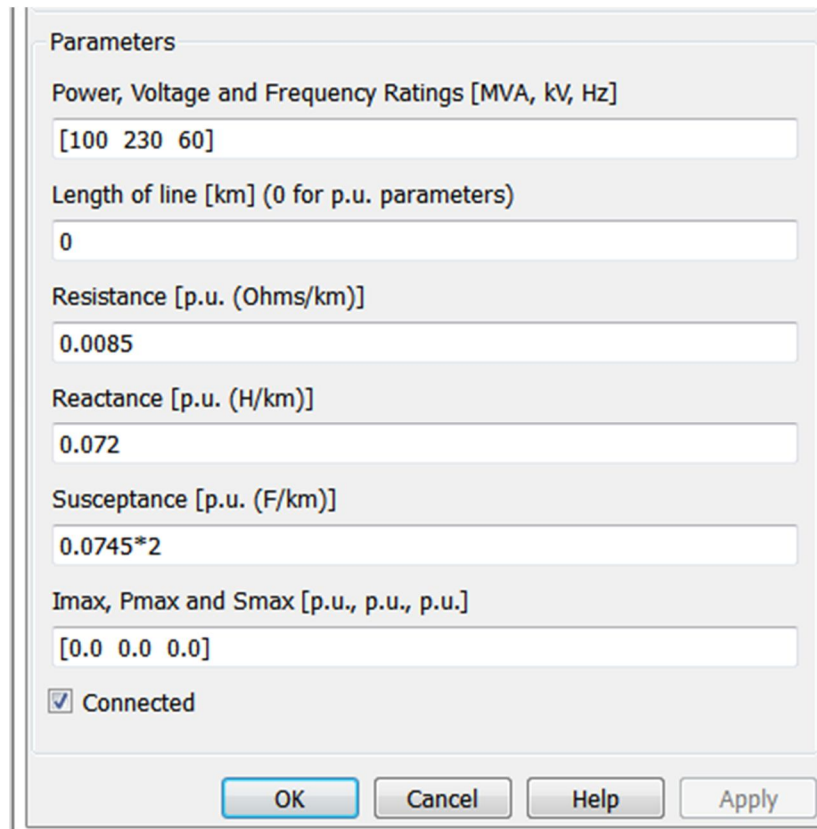


Figure 4.1: WSCC 9-bus test system.

In this thesis, the Western System Coordinating Council (WSCC) 9-bus test system shown in Fig.4.1 is used. The test system data is given in the Appendix A. Bus 1 is considered as slack bus. Two synchronous generators which supply a real power output of 1.63 pu and 0.85 pu are connected at bus 2 and bus 3, respectively. The system has 3-loads connected at bus 5, bus 6 and bus 8. Generators are modeled as PV bus. Figure 4.2 shows the block parameters of pi model of the transmission line connecting bus 7 and 8. The PV bus parameters for G2 is shown

in Fig. 4.3. As FACTS device, a static var compensator (SVC) and a static synchronous compensator (STATCOM) are used in the analysis [37].



The image shows a software dialog box titled "Parameters" for configuring transmission line settings. The dialog contains several input fields and a checkbox, all set within a light gray frame. At the bottom, there are four buttons: "OK", "Cancel", "Help", and "Apply".

Parameter	Value
Power, Voltage and Frequency Ratings [MVA, kV, Hz]	[100 230 60]
Length of line [km] (0 for p.u. parameters)	0
Resistance [p.u. (Ohms/km)]	0.0085
Reactance [p.u. (H/km)]	0.072
Susceptance [p.u. (F/km)]	0.0745*2
Imax, Pmax and Smax [p.u., p.u., p.u.]	[0.0 0.0 0.0]
Connected	<input checked="" type="checkbox"/>

Figure 4.2: Transmission line parameters.

Block Parameters: PV

PV (mask)

This block defines a PV bus for load flow studies:

$P = P_{cost}$
 $V = V_{des}$

Parameters

Power and Voltage Ratings [MVA, kV]

Active Power [p.u.]

Voltage Magnitude [p.u.]

Qmax and Qmin [p.u. p.u.]

Vmax and Vmin [p.u. p.u.]

Loss Participation Factor

Connected

OK Cancel Help Apply

Figure 4.3: PV bus parameters.

4.2.2 Static Voltage Stability Analysis

A load flow study for the considered test system is conducted using Newton-Raphson method [46]. The bus voltage of the system without FACTS (base case) is shown in Fig.4.4. From this Figure it can be seen that the bus 5 has the lowest voltage magnitude compared to other buses. To analyze the static voltage stability generally power-voltage (P-V) curves are used which determine the maximum loading limit of a system [2]. Here, this curve has been produced by using a series of power flow solutions using power system analysis toolbox (PSAT) for different load levels. Initially, a SVC and a STATCOM of same the capacity is connected at bus 8 separately for a comparative analysis.

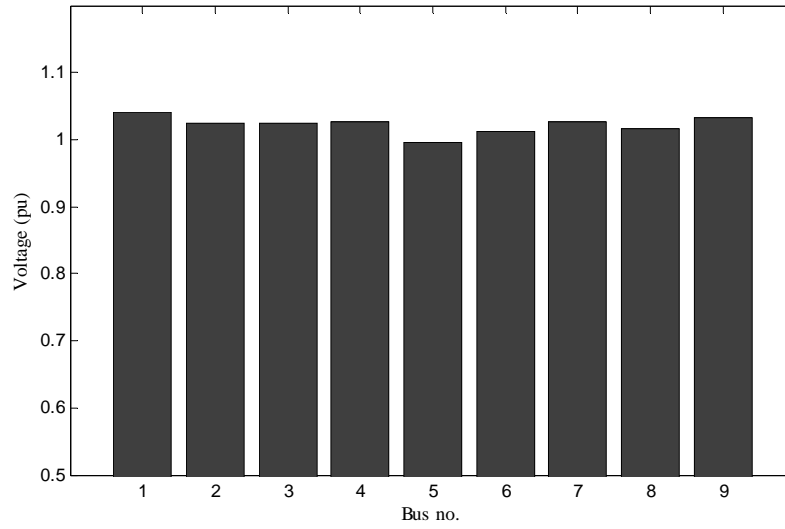


Figure 4.4: Bus voltages of the system.

The variations in load bus voltages with the loading factor are obtained and summarized in Table 4.1 from which it can be seen that a FACTS device can improve the maximum loading point (MLP) of the system. The base case P-V curve for all the buses is shown in Fig. 4.5. The improvement in the MLP for the connection of a FACTS device can be easily visualized from Figures 4.6 and 4.7.

A STATCOM has superior performance in improving MLP of the system due to its inherent control capability. For this reason, the rest of the analysis of this thesis is carried out with a STATCOM.

Table 4.1: MLP with and without FACTS device

Name of FACTS device	Maximum loading point (MLP), (pu)
Base case	2.6407
SVC	2.7323
STATCOM	2.9030

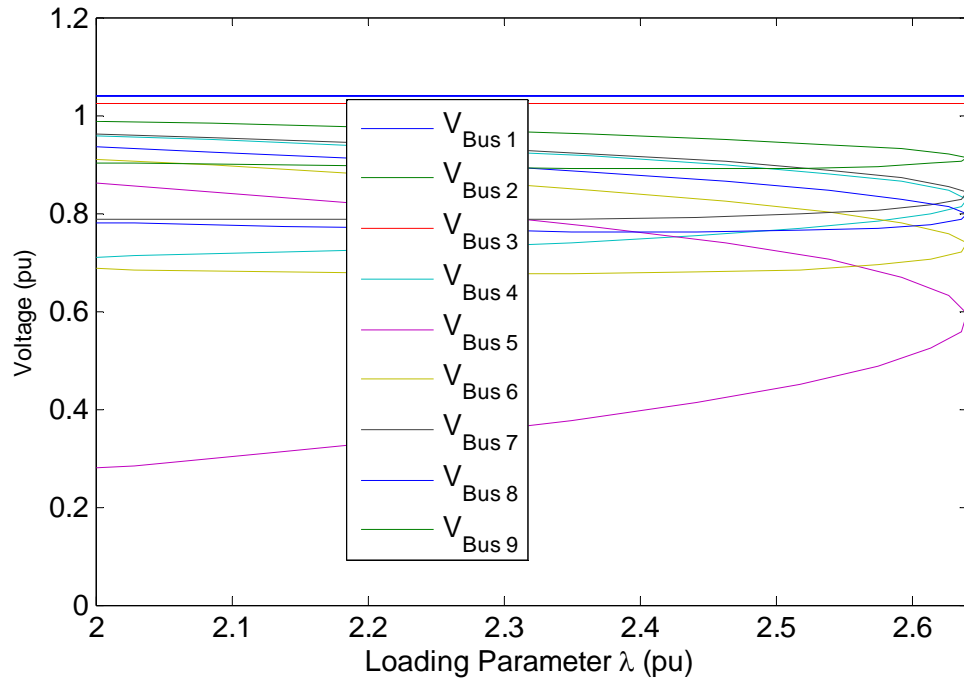


Figure 4.5: P-V curve without FACTS device.

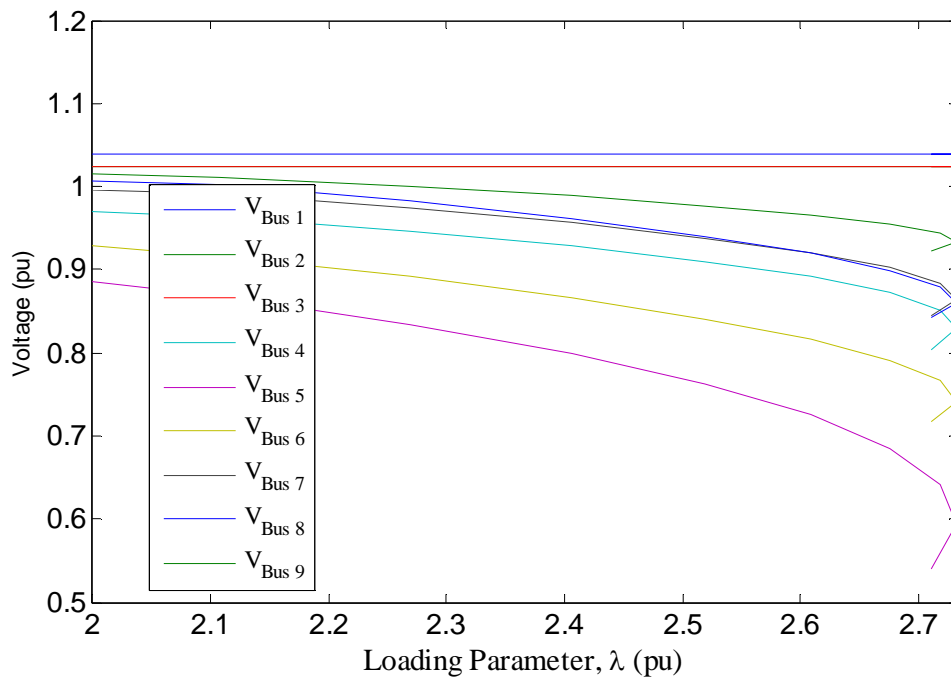


Figure 4.6: P-V curve with SVC installed at bus 8.

In order to investigate the impact of location of FACTS on the network, a STATCOM is placed in different load buses; and MLP and power losses are calculated for each case. From Table 4.2, it can be seen that the connection of a STATCOM at the weakest bus increases the MLP and power loss compared to its connection at other load buses. As the weakest bus in a system requires the most reactive power, placing a STATCOM at this bus can improve loading margin the most.

Table 4.2: MLP and power loss for connection of STATCOM at different load buses

Load bus no.	MLP (pu)	Power loss (pu)
Bus 5	3.4477	0.04497
Bus 6	2.6651	0.04618
Bus 8	2.9086	0.04587

Therefore, to reduce the possibility of voltage collapse and power loss, the weak bus is the best choice to install an expensive FACTS device. The voltage profile of the system with a STATCOM connected at bus 5 is shown in Fig. 4.8 from which it can be seen that the installation of STATCOM at the weakest bus improves the voltage profile of the system significantly compared to the base case.

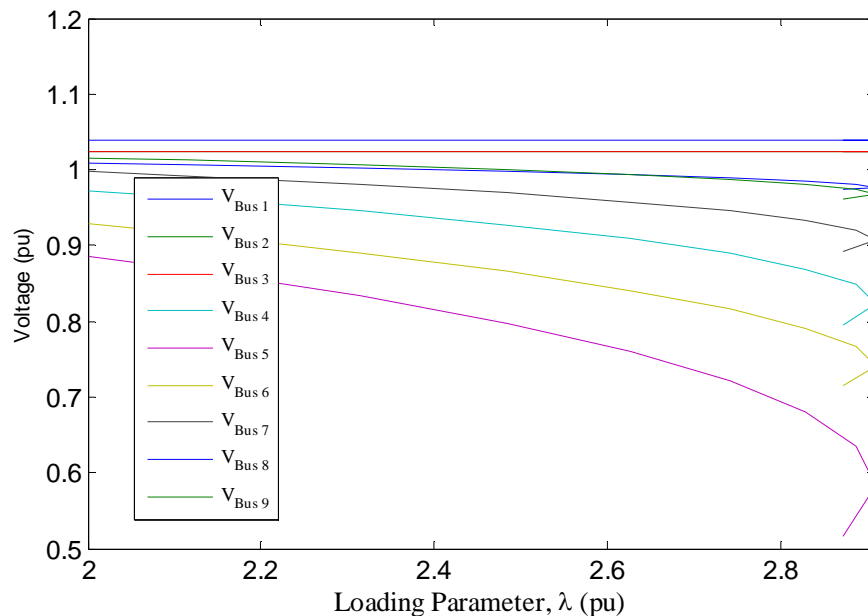


Figure 4.7: P-V curve with STATCOM installed at bus 8.

synchronous compensators. All the loads are considered as constant impedance loads and mechanical inputs to the generators are assumed to be constant. A sixth order model of the synchronous generator is used for the analysis. The test system data is given in Appendix B.

The equations governing the generator dynamics are given below [37].

$$\dot{\delta} = \Omega_b(\omega - 1) \quad (4.1)$$

$$\dot{\omega} = (p_m - p_e - D(\omega - 1))/M \quad (4.2)$$

$$\dot{e}'_q = (-f_s(e'_q) - \left(x_d - x'_d - \frac{T''_{do}x''_d}{T'_{do}x'_d} (x_d - x'_d) \right) i_d + \left(1 - \frac{T_{AA}}{T'_{do}} \right) v_f)/T'_{do} \quad (4.3)$$

$$\dot{e}'_d = (e'_d) - \left(x_q - x'_q - \frac{T''_{qo}x''_q}{T'_{qo}x'_q} (x_q - x'_q) \right) i_q/T'_{qo} \quad (4.4)$$

$$\dot{e}''_q = (-e''_q + e'_q) - \left(x'_d - x''_d + \frac{T''_{do}x''_d}{T'_{do}x'_d} (x_d - x'_d) \right) i_d + \left(1 - \frac{T_{AA}}{T'_{do}} \right) v_f/T''_{do} \quad (4.5)$$

$$\dot{e}''_d = (-e''_d + e'_d) - \left(x'_q - x''_q + \frac{T''_{qo}x''_q}{T'_{qo}x'_q} (x_q - x'_q) \right) i_q/T''_{qo} \quad (4.6)$$

$$\text{The electric power, } p_e = (v_q + r_a i_q) i_q + (v_d + r_a i_d) i_d \quad (4.7)$$

The algebraic constants are as follows:

$$0 = v_q + r_a i_q - e''_q + x''_d i_d \quad (4.8)$$

$$0 = v_d + r_a i_d - e''_d + x''_q i_q \quad (4.9)$$

where, f_n refers to frequency, r_a armature resistance, x''_d , x'_d , and x_d are the direct axis sub-transient, transient and synchronous reactance, respectively, x''_q , x'_q , and x_q are the quadrature axis sub-transient, transient and synchronous reactance, respectively, T''_{do} , T'_{do} are the d-axis open circuit sub-transient and transient time constant, respectively, T''_{qo} , T'_{qo} are the q-axis open circuit sub-transient and transient time constant, respectively, M inertia constant, D damping coefficient, Ω_b base frequency in rad/s, ω rotor speed, T_{AA} is d-axis additional leakage time constant, v_f excitation voltage, p_m mechanical power input, p_e output electrical power, i_q and i_d are the d-axis and q-axis current, respectively. All the values of model parameters are given in Appendix C. Fig. 4.10 shows the model parameters of generator connected at bus 2.

Block Parameters: Gen3

Parameters

Power, voltage and frequency ratings [MVA, kV, Hz]
[60 69 60]

Machine Dynamic Order 6

resistance r_a and leakage reactance x_l [p.u. p.u.]
[0.0031 0.00]

d-axis reactances X_d , X'_d X''_d [p.u.,p.u.,p.u.]
[1.05 0.1850 0.13]

d-axis open circuit time constants T'_{d0} and T''_{d0} [s, s]
[6.1 0.04]

q-axis reactances X_q , X'_q , X''_q [p.u. p.u. p.u.]
[0.98 0.36 0.13]

q-axis open circuit time constants T'_{q0} and T''_{q0} [s s]
[0.3 0.099]

Inertia ($M = 2H$) and Damping [s, p.u.]
[2*6.54 2.00]

Speed and active power additional signals K_w K_p [p.u., p.u.]
[0.00 0.00]

OK Cancel Help Apply

Figure 4.10: Model parameters of generator connected at bus 2.

A STATCOM is used as a Flexible AC Transmission System (FACTS) device in this analysis (Fig. 2.4). This STATCOM is equipped with a power oscillation damping (POD) controller as shown in Fig. 4.11 which contains gain, wash-out and compensator blocks.

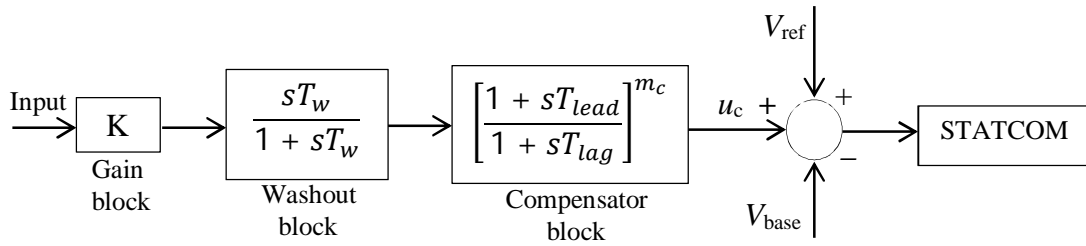


Figure 4.11: STATCOM with POD controller

4.3.2 Static and Dynamic Analysis

To analyze the static voltage stability generally real power-voltage (P-V) or reactive power-voltage (Q-V) curves are used which determine the maximum loading limit of a system [2], [53]. Here, P-V curve has been produced by using a series of power flow solutions (continuation power flow) using power system analysis toolbox (PSAT) in MATLAB environment for different load levels.

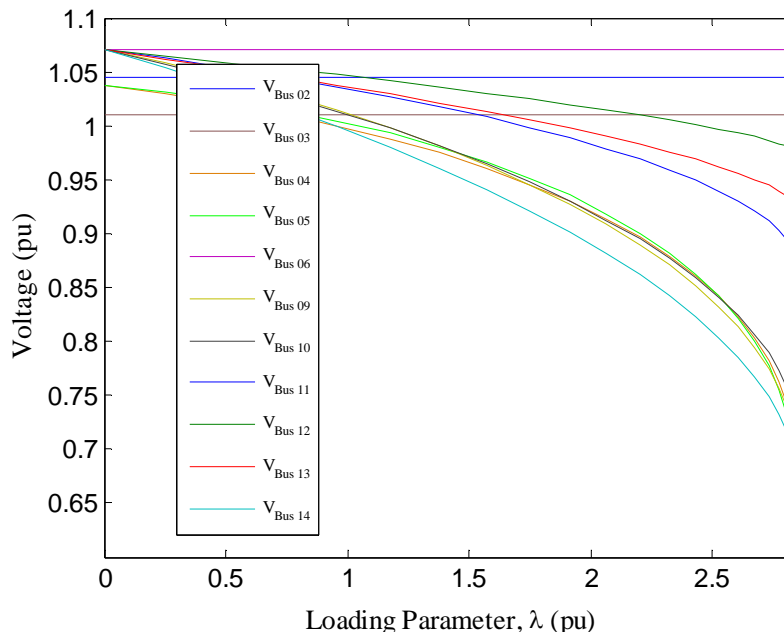


Figure 4.12: Loading parameter-voltage curve under base case.

The variations in load bus voltages with the loading factor are obtained and plotted in Fig. 4.12 from which it can be observed that bus-14 is the weakest bus of this network. In this thesis, a STATCOM is installed at bus-14 to enhance the static voltage stability of the system.

Next, to understand the inherent dynamics of the system, the test system is linearized and eigenvalues are calculated without STATCOM connection. The linearized system can be represented by the following equations [2]:

$$\Delta x = A\Delta x + B\Delta u \quad (4.10)$$

$$\Delta y = C\Delta x + D\Delta u \quad (4.11)$$

where, A represents system matrix, B represents input matrix, C represents output matrix, x represents states, y represents output and u is the input.

The transfer function of a system can be written as

$$G(s) = \frac{\Delta y(s)}{\Delta u(s)} = C(sI - A)^{-1}B \quad (4.12)$$

The eigenvalues of a matrix are given by the values of the scalar parameters λ for which there exist non-trivial solutions (i.e., other than $\phi=0$) to the equation

$$A\phi = \lambda\phi \quad (4.13)$$

To find the eigenvalues, the above equation may be written in the form

$$(A - \lambda I)\phi = 0 \quad (4.14)$$

Characteristic equation, $\det(A - \lambda I) = 0$, where λ is the eigenvalue of A .

For a complex pair of eigenvalues, $\lambda_i = \sigma_i \pm j\omega_i$, the frequency of oscillation is given by

$$f = \frac{\omega}{2\pi} \quad (4.15)$$

The damping ration is given by

$$\xi = \frac{-\sigma}{\sqrt{\sigma^2 + \omega^2}} \quad (4.16)$$

For any eigenvalue λ_i , the n-column vector ϕ_i which satisfy equation (4.6) is called is called the right eigenvector of A .

$$A\phi_i = \lambda_i\phi_i, i=1,2,\dots,n \quad (4.17)$$

Similarly, the n-row vector ψ_i which satisfies

$$\psi_i A = \lambda_i\psi_i, i=1,2,\dots,n \quad (4.18)$$

is called the left eigenvector.

The element $P_{ki} = \phi_{ki}\psi_{ik}$ is termed as participation factor. It is a measure of the relative participation of the k^{th} state variable in the i^{th} mode and vice versa.

$G(s)$ can be expanded in partial fractions of the Laplace transform of y , in terms of C and B matrices and the left and right eigenvectors as [2]:

$$G(s) = \sum_{i=1}^n \frac{C\phi(:,i)\psi(i,:)B}{(s-\lambda_i)} = \sum_{i=1}^n \frac{R_i}{(s-\lambda_i)} \quad (4.19)$$

Here, R_i is called residue of mode i which gives the measure of that mode's sensitivity to a feedback between the output y and input u .

When applying the feedback control $H(s)$, eigenvalues of the initial system $G(s)$ are changed and the shift of an eigenvalue is calculated by:

$$\Delta\lambda_i = R_i H(\lambda_i) \quad (4.20)$$

It is found that the system has a pair of eigenvalue at $-0.04654 \pm 8.1151j$ which is the critical mode of this system. Table 4.3 shows the participation factors of the dominant states associated with this mode, where $e1q_Syn_1$ and vf_Exc_1 represents the quadrature axis voltage of synchronous machine 1 and voltage of the exciter 1, respectively; δ_Syn_1 and ω_Syn_1 represents the angle and speed of the generator 1, respectively. This mode has a damping ratio of 0.57%. It is known that the minimum damping requirements for reliable operation of power system is 5%.

Table 4.3: Critical mode of the considered system

Critical mode	Dominant States and participation factor	Damping ratio (%)
$-0.04654 \pm 8.1151j$	$e1q_Syn_1=0.22377, vf_Exc_1=0.17139$ $\delta_Syn_1=0.04332, \omega_Syn_1=0.04332$	0.57

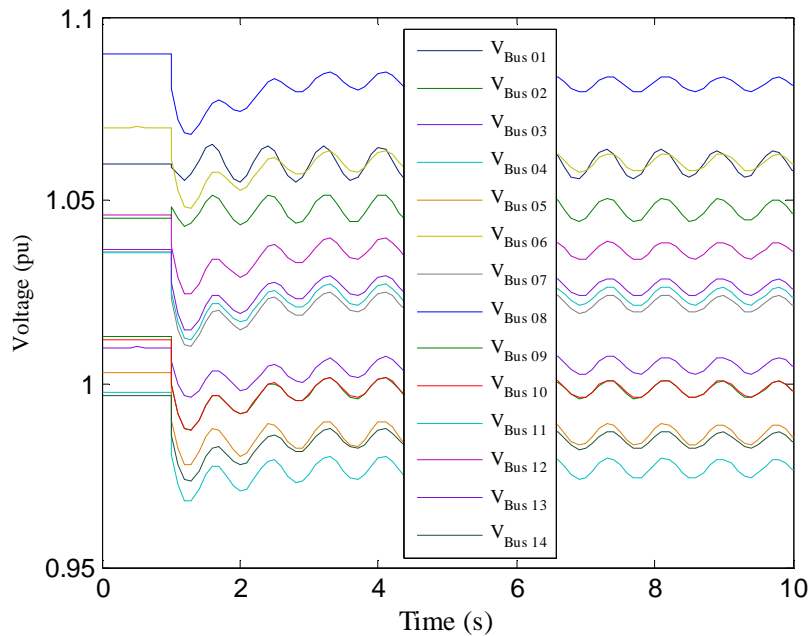


Figure 4.13: Bus voltages of IEEE 14-bus test system under disturbance.

To test the dynamic performance of the system, the line between bus 2 and bus 4 is disconnected at 1s. Fig. 4.13 shows the bus voltage profile of the system from which it can be seen that the system suffers from low frequency oscillations. The real power of the synchronous generator is shown in Fig. 4.14. In this analysis, mechanical input to the generator is kept constant. It can be seen from Fig. 4.14 that the system has large oscillations in its output power.

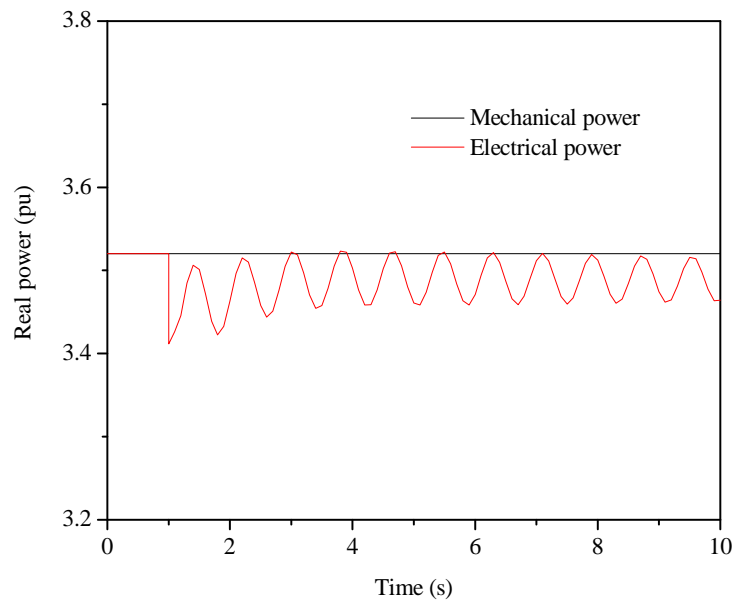


Figure 4.14: Mechanical input power and electrical output power of synchronous generator 1.

4.3.3 Proposed Methodology

To solve the above problems, a STATCOM is connected and linear analysis is carried out. It is found that it cannot improve the damping ratio to the acceptable level. Therefore, a POD controller is equipped with it based on the line active power measurement from bus 1. The transfer function of the POD controller is given below [54].

$$H(s) = K \frac{sT_w}{sT_w + 1} \left[\frac{sT_{lead} + 1}{sT_{lag} + 1} \right]^{m_c} = KH_1(s) \quad (4.21)$$

$$\varphi_{comp} = 180^\circ - \arg(R_i) \quad (4.22)$$

$$\alpha_c = \frac{T_{ld}}{T_{lg}} = \frac{1 - \sin\left(\frac{\varphi_{comp}}{m_c}\right)}{1 + \sin\left(\frac{\varphi_{comp}}{m_c}\right)} \quad (4.23)$$

$$T_{lg} = \frac{1}{\omega_i \sqrt{\alpha_c}}, \quad T_{ld} = \alpha_c T_{lg} \quad (4.24)$$

$$K = \left| \frac{\lambda_{i,des} - \lambda_i}{R_i H_1(\lambda_i)} \right| \quad (4.25)$$

where, the phase angle φ_{comp} shows the compensation angle needs to move the eigenvalue direct to the left parallel with the real axis. T_w, T_{ld} and T_{lg} are the time constant of the wash-out, lead and lag block, respectively, $\lambda_{i,des}$ is the desired eigenvalue, $\arg(R_i)$ is the phase angle of the residue R_i , ω_i , m_c and K is the frequency of the mode of oscillation in rad/s., number of compensation stages and the controller gain, respectively. In this paper, number of compensation stages are 2. The implemented model of the IEEE 14-bus test system is shown in Fig 4.15.

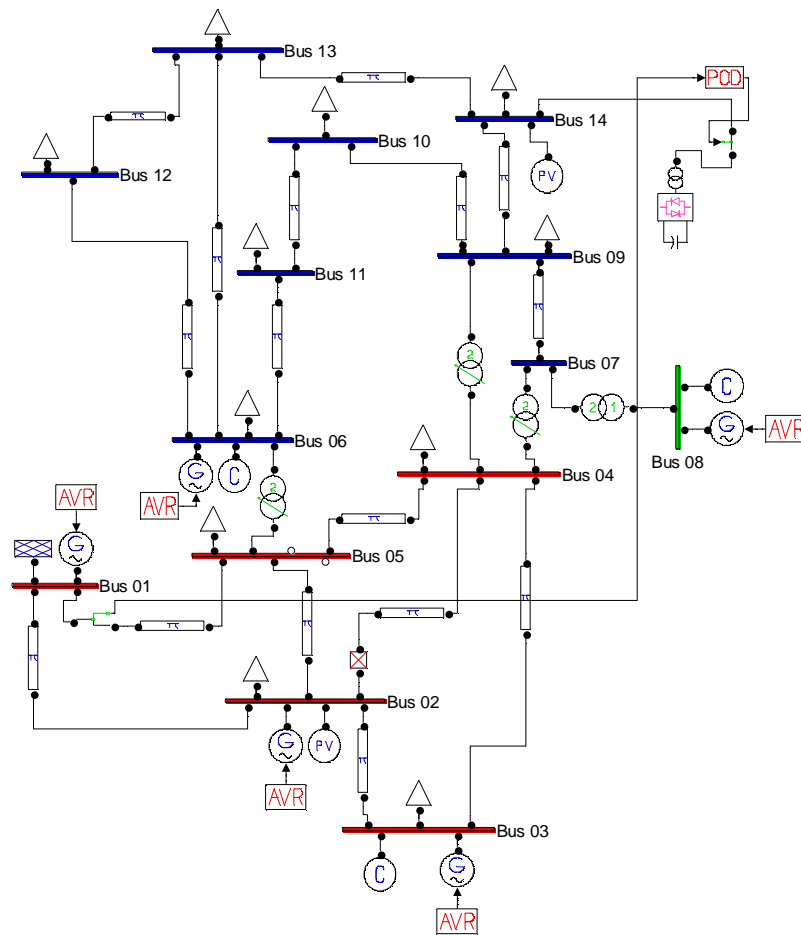


Figure 4.15: Implemented PSAT model of IEEE 14-bus test system with STATCOM and POD controller.

The overall design step is described below:

Step1: Run continuation power flow routine and identify the weakest bus of the system.

Step2: Find the eigenvalues of the system and observe the oscillatory modes.

Step3: Place a STATCOM in the weakest bus.

Step4: Perform linear analysis and identify the critical eigenvalue (λ_i).

Step5: Calculate residue (R_i), T_{ld} and T_{lg} .

Step6: Select washout time constant which is in the range of 5-10s.

Step7: Determine constant K from equation (4.25)

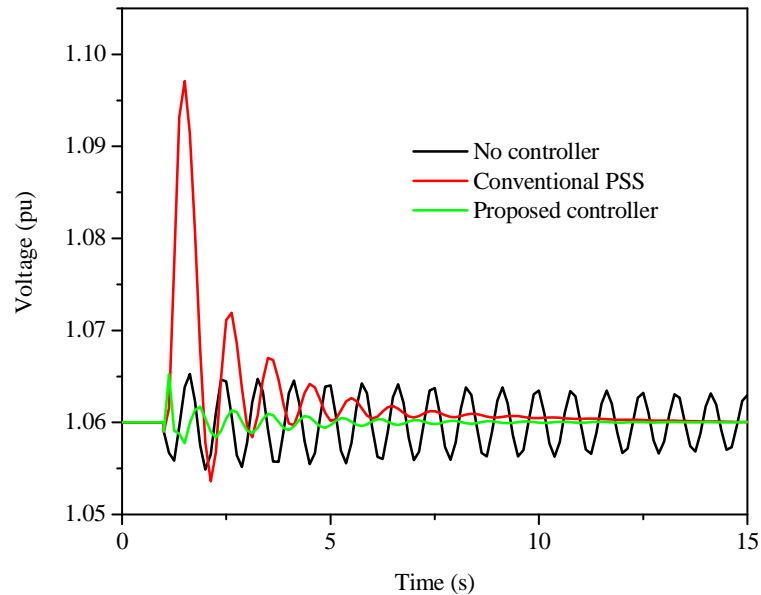


Figure 4.16: Bus 1 Voltage

For this test system, $|R_i|=0.66$, $T_{ld}=0.0508$, $T_{lg}=0.298$, $T_w=5$ and the constant gain K is 0.40. The desired eigenvalue is $-0.7216 \pm 8.1151j$ which has a damping ratio of 8.8%.

For a comparative purposes, the system is also simulated with the conventional PSS [37] which is usually used to improve the damping of oscillatory mode. The voltage profile of the test system at bus 1 without damping controller, PSS and with the proposed damping controller is shown in Fig. 4.16 from which it can be clearly observed that the proposed control scheme damps the oscillations quickly. It has also less overshoot compared to the system with conventional PSS. The dominant eigenvalue of the system with the proposed controller is $-0.6402 \pm 7.6527j$ with a damping ratio 8.3% which is greater than the minimum limit (5%).

4.4 Summary

This chapter describes the assesment of power system static voltage stability with FACTS devices and the improvement of oscillation damping using STATCOM. A STATCOM performs better than an SVC not only to ensure static voltage stability of the power system but also to enhance oscillation damping performance significantly when equipped with a POD controller.

CHAPTER V

Frequency Stability Improvement during Cyber-Attack

5.1 Introduction

Load of a power station is always varying in nature. The frequency of the alternator changes with the change in load of a power station. The frequency sensor senses the system frequency and according to the signal from frequency sensor the LFC sets the prime mover speed to compensate the system frequency. In this work, speed regulation is identified as the vulnerable quantity. Malfunctioning of the governor speed regulator due to cyber-attack causes the speed of the prime mover out of control and results in making the system frequency unstable.

For proper operation of AGC, appropriate value selection of integral controller gain (K_I) is important. Improper selection of the value of K_I leads to malfunction of governor to set appropriate point to restore the system frequency. This thesis work identifies K_I as the other vulnerable quantity of cyber- attack. Any change of K_I due to unauthorized access to AGC loop may cause the system frequency oscillation which disturbs the system stability.

In this work, cyber-attack is classified into two types, one is positively biased attack and the other one is negatively biased attack depending on the affected value of speed regulation (R) and integral controller gain (K_I).

5.2 Cyber-Attack Impact on LFC

For stable operation of power system proper operation of LFC is important. However, it may be vulnerable due to cyber-attack.

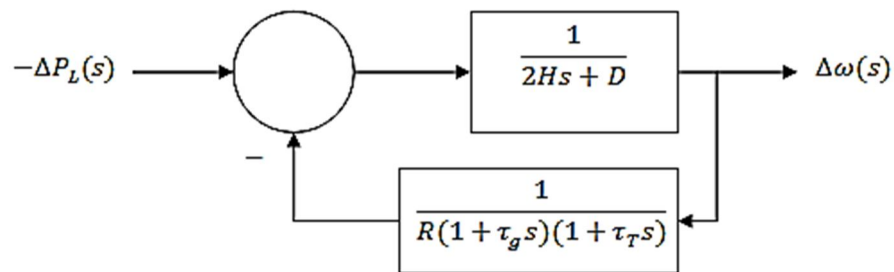


Figure 5.1: Equivalent block diagram of LFC

It is assumed first that the control system is not attacked by unauthorized people. In this condition if sudden load change (load increases) occurs, the system frequency will fall below the nominal frequency for a short instant of time. The frequency sensor senses the fall of the system frequency and sends signals to the LFC for proper speed regulation. According to the signals from frequency sensor the LFC sets the governor speed regulation to compensate the prime mover speed and stables the system frequency. It will possible only for the proper setting of the governor speed regulation.

Due to cyber-attack, LFC may not be able to set the regulation properly and if this occurs then the system frequency will oscillate and make the system unstable.

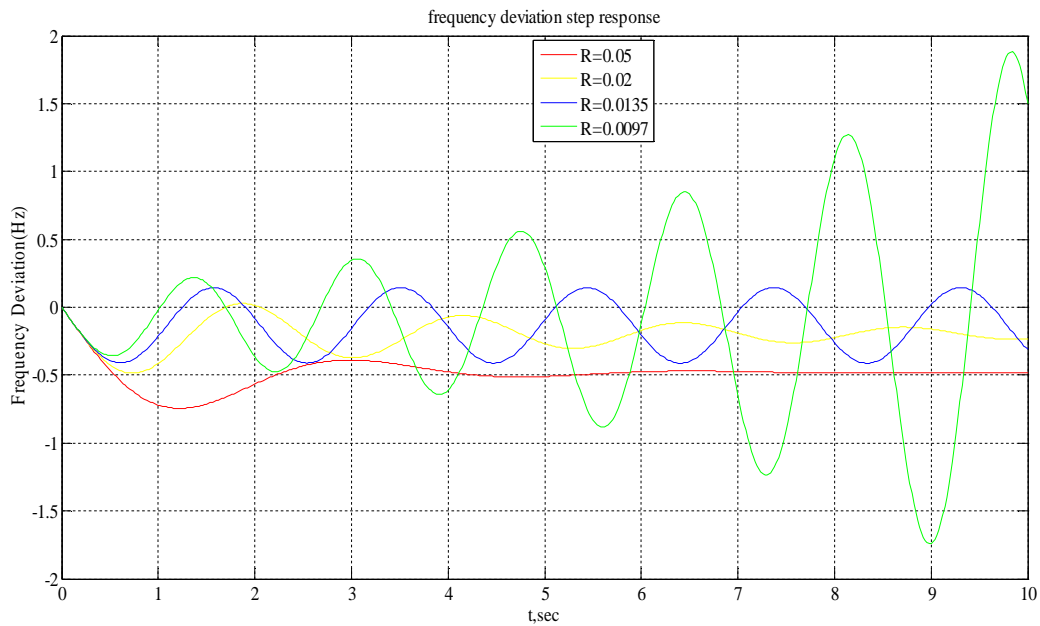


Figure 5.2: System Frequency deviation under different values of speed regulation.

The stable limit of speed regulation (R) can be derived from the characteristic equation of LFC loop using Routh-Hurwitz array. The simplified block diagram [52] of LFC system is shown in Fig. 5.1.

$$\frac{\Delta\Omega(s)}{-\Delta P_L(s)} = \frac{(1 + \tau_g s)(1 + \tau_T s)}{(2Hs + D)(1 + \tau_g s)(1 + \tau_T s) + 1/R} \quad (5.1)$$

This thesis considers an islanded power station that has the following parameters with 250MW turbine output power at a nominal frequency of 50Hz and a sudden load change of 50MW [52].

From equation (5.1), using the power system parameters of Table 5.1 and Routh-Hurwitz array, the stability limit of speed regulation is obtained as $R > 0.0135$ (Art. 3.1.6).

Table 5.1: Power system parameters

Parameter	Value
Turbine time constant (τ_T)	0.2 sec
Governor time constant (τ_g)	0.5 sec
Generator inertia constant (H)	5.0 sec
Variation of load for 1% change in frequency (D)	0.8

From Fig. 5.2 it is seen that when $R=0.05$, the system frequency deviation is in stable condition. So for stable operation of this power station the set value of R should be 0.05. The Matlab code for Fig. 5.2 can be found in Appendix D.1. Any deviation from this set value results the system frequency deviation unstable. The instability of system frequency deviation makes the governor incapable of compensating the frequency deviation i.e. the system frequency will not be restored in case of sudden load change. The deviation of speed regulation from set value is due to cyber- attack on LFC (Unauthorized access to the control of LFC).

5.2.1 Result of Positively Biased Attack

Positively biased attack is caused when the value of speed regulation increases due to cyber-attack. From Fig. 5.3, it is clear that in case of positive bias the system frequency can be restored without disturbing the stability of the system frequency. But too much deviation of system frequency may allow the governor to take more time to set the desired position to restore the system frequency.

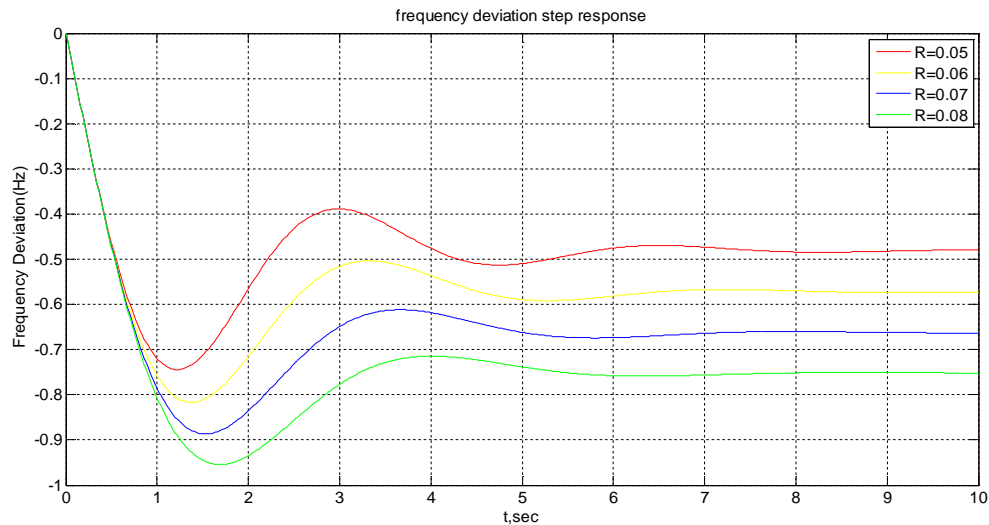


Figure 5.3: Frequency deviation in case of positively biased attack.

5.2.2 Result of Negatively Biased Attack

The decreasing of speed regulation value due to cyber-attack is termed as negative biased attack. Due to attack, if the speed regulation value falls below the stable condition ($R > 0.0135$), the frequency deviation will be oscillating in nature and governor fails to restore the system frequency as shown in Fig. 5.4. Hence, negatively biased cyber-attack is the major challenge for engineers to maintain the system frequency in stable condition during sudden change of load of the system. The Matlab code for Fig. 5.3 and Fig. 5.4 can be found in Appendix D.2 and Appendix D.3 respectively.

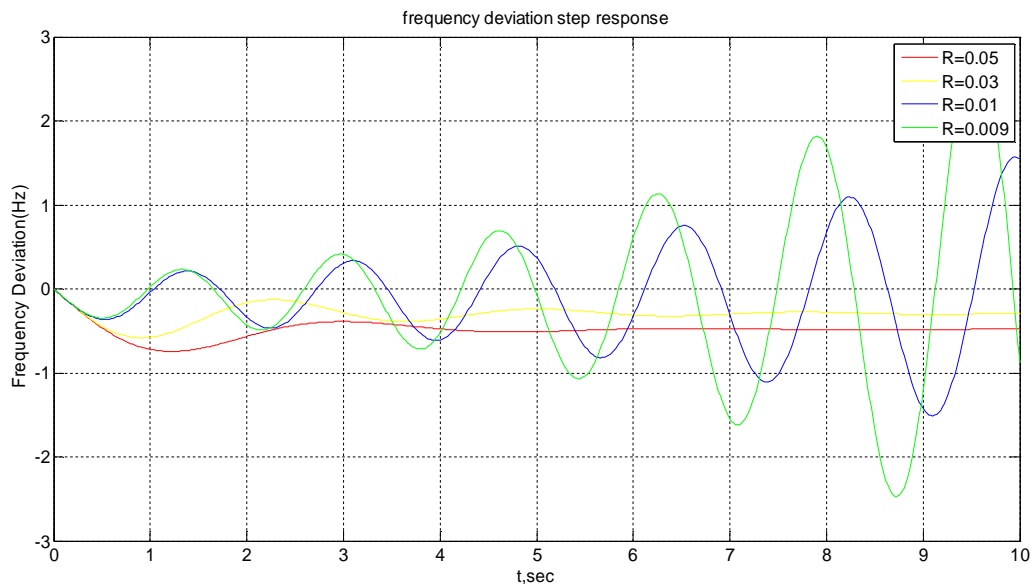


Figure 5.4: Frequency deviation in case of negatively biased attack.

5.3 Cyber-Attack Impact on AGC

With the primary LFC loop, a change in the system load will result in steady state frequency deviation, depending on governor speed regulation. The primary LFC loop takes a considerable time to restore system frequency that is not allowable. In order to reduce the frequency deviation to zero a modification is needed to LFC. The modification can be achieved by introducing an integral controller to act on the load reference setting to change the speed set point. The integral controller increases the system type by 1 which forces the final frequency deviation to zero.

The LFC system, with the addition of secondary loop (integral controller) is the Automatic Generation Control (AGC). The integral controller gain K_I must be adjusted for satisfactory transient response. The addition of integral controller in parallel with LFC allows the governor

to set appropriate point to increase speed of turbine in case of sudden load rise and to restore the system frequency quicker than primary LFC loop.

Appropriate value of K_I is determined using the characteristics equation of AGC loop. The equivalent diagram [52] of AGC is shown in Fig. 5.5, from which the closed loop transfer function is obtained.

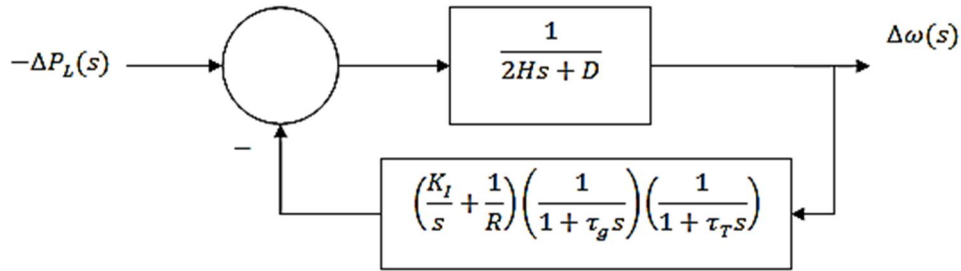


Figure 5.5: The equivalent block diagram of AGC

The closed loop transfer function of the control system shown in Fig. 5.5 is

$$\frac{\Delta\Omega(s)}{-\Delta P_L(s)} = \frac{(1 + \tau_g s)(1 + \tau_T s)}{(2HS + D)(1 + \tau_g s)(1 + \tau_T s) + K_I + s/R} \quad (5.2)$$

Fig. 5.6 shows the frequency deviation step response to determine the right value of K_I at which frequency deviation is zero. Its Matlab code is shown in Appendix D.4.

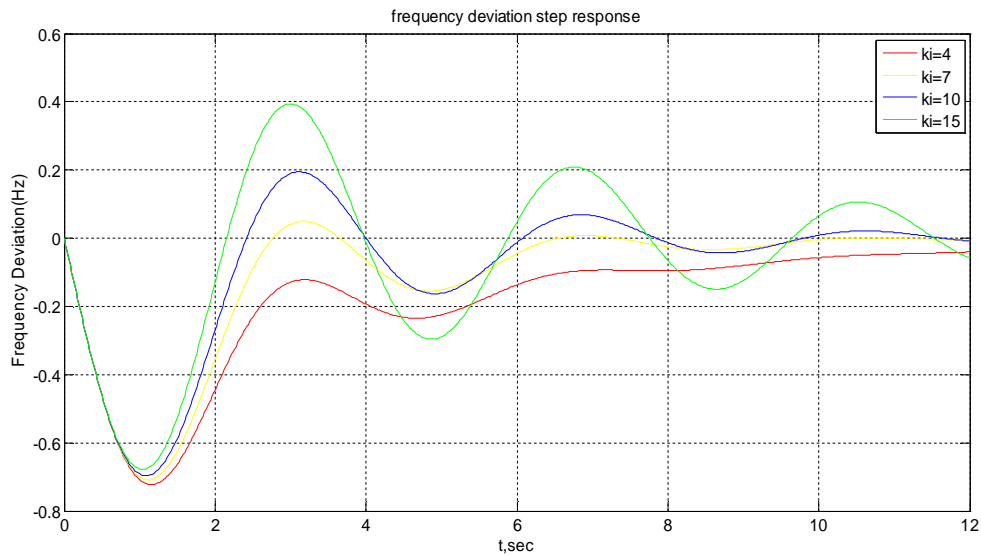


Figure 5.6: Frequency deviation step response for different values of K_I .

From the above figure it is seen that for $K_I=7$ the deviation comes to zero position quicker than the other K_I values. That is why we can chose $K_I=7$ for proper operation of AGC.

The attack on AGC may lead to the malfunctioning of AGC that causes the system frequency deviation from nominal frequency and also makes the oscillation of frequency deviation. Seriousness of the effect of attack depends on the type of attack (positive biased or negative biased). This work defines the rise of the value of K_I as positively biased attack and the falling down of the value of K_I as negatively biased attack.

5.3.1 Positively Biased Attack

Unauthorized access to AGC control may lead to the system frequency deviation and sometimes make the deviation oscillating in nature. If the system frequency deviation is unstable, it will be impossible for governor to restore the system frequency. Moreover the attack on AGC may cause unwanted delay to restore system frequency.

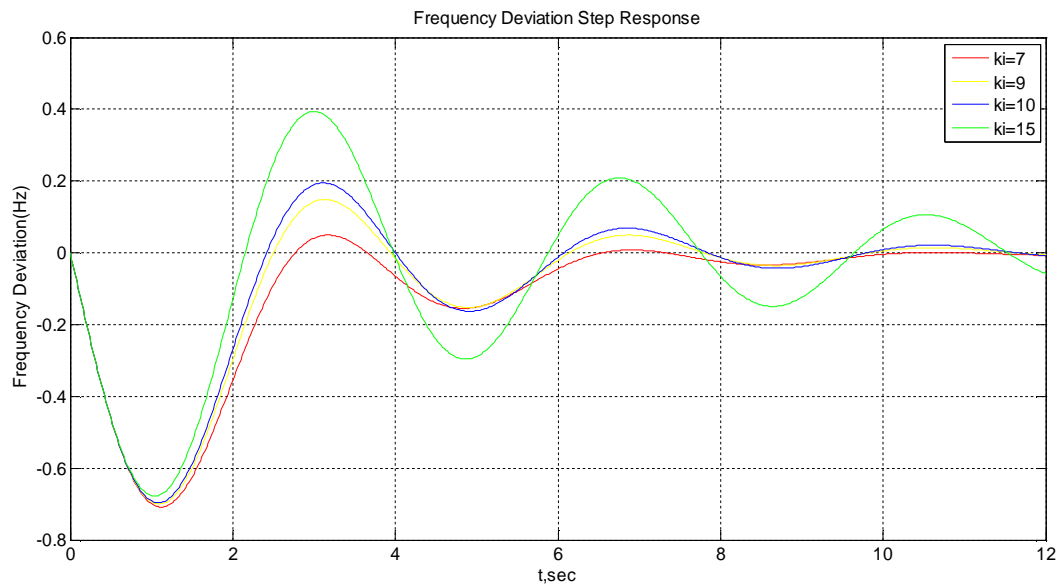


Figure 5.7: Frequency deviation due to positively biased attack.

In Fig. 5.7, the effect of positively biased attack on AGC is shown and the red curve is the set value under unaffected condition. The yellow curve means that there is slight frequency deviation from the set condition (Red curve). This leads to unwanted delay to restore the system frequency. The blue curve indicates that the frequency deviation is slightly oscillating in nature.

The oscillation of the frequency deviation leads to the instability of system frequency. Due to this oscillation, the governor will fail to set the appropriate point to restore the system frequency. The deviation of oscillation in green curve is higher that indicates serious attack on

AGC and the governor will no longer be able to restore the system frequency. More the positive biased attack is occurred, more serious the impact on system frequency is appeared.

5.3.2 Negatively Biased Attack

The seriousness of the attack on AGC depends on the type of attack. Negatively biased attack means the falling down of the value of K_I from the set value due to unauthorized access to AGC system. This attack may oppose the objectives of the use of integral controller with primary loop of LFC to obtain AGC system to reduce the frequency deviation to zero. The result of negatively biased attack on AGC is shown in Fig. 5.8.

The primary LFC control loop is modified to form AGC to reduce the frequency deviation to zero. From Fig. 5.8 it is clear that due to negative biased attack, frequency is deviated from nominal frequency.

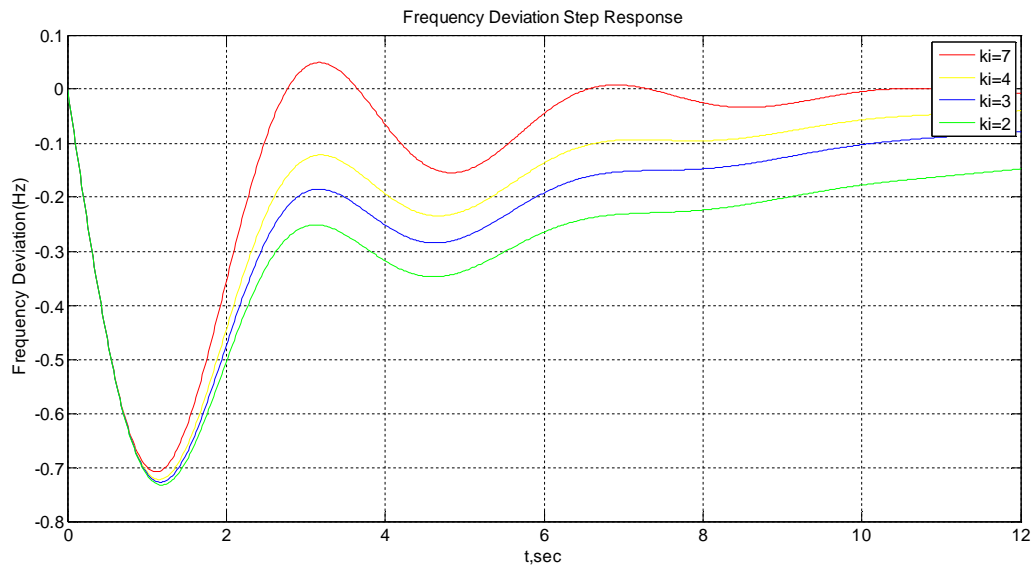


Figure 5.8: Frequency deviation due to negatively biased attack.

It leads to the unwanted delay of restoring the system frequency. Negative biased attack on AGC is not so serious like positive one because it does not make the frequency deviation oscillating in nature. Appendix D.5 and Appendix D.6 describes the Matlab code of Fig 5.7 and Fig. 5.8. Impact of cyber attack on LFC and AGC of a power station is summarized in Fig. 5.9.

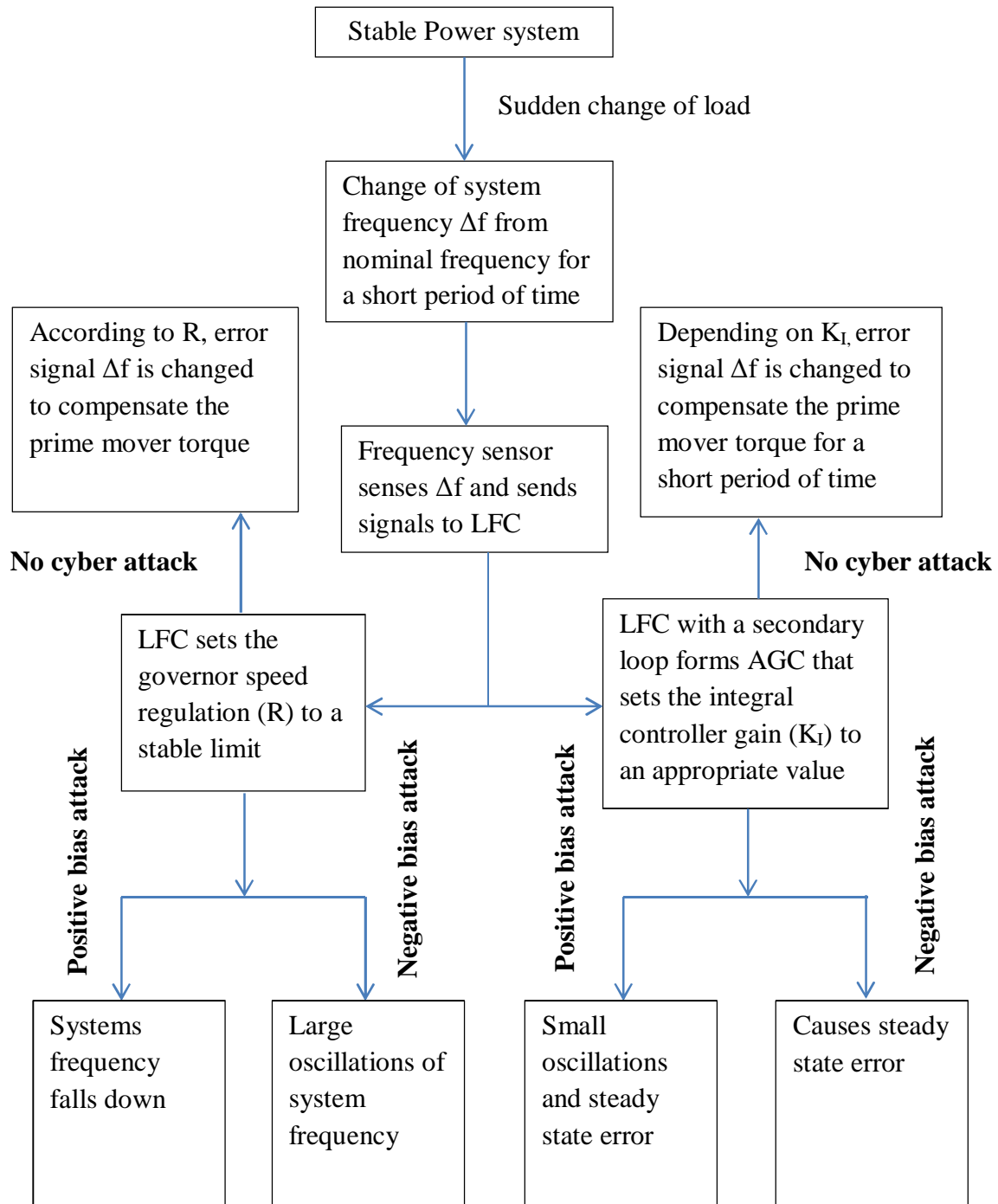


Figure 5.9: Cyber attack impact on LFC and AGC at a glance.

5.4 Mitigation of Frequency Disturbance

5.4.1 Effect of Sudden Load Change

When the load of an alternator is changed, the speed of the prime mover also changes accordingly maintaining Lenz's law. If the load increases, the speed of the prime mover decreases and vice versa.

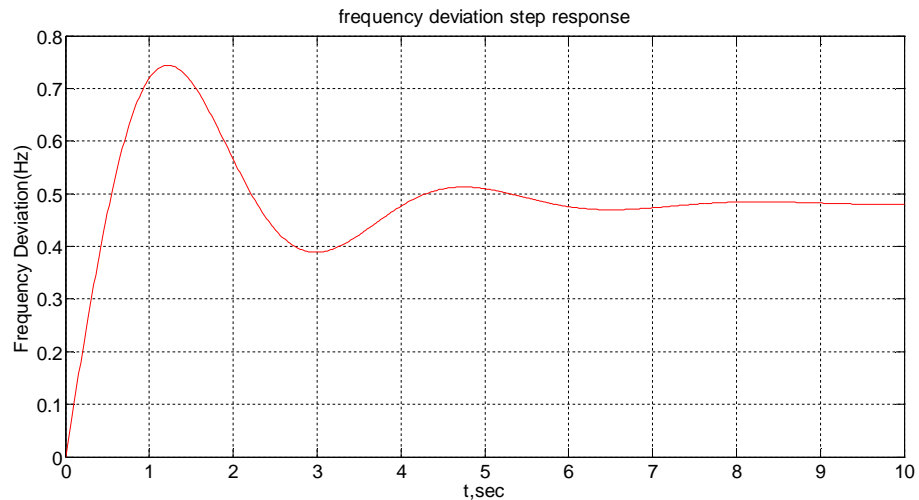


Figure 5.10: Frequency deviation step response (sudden load decrease).

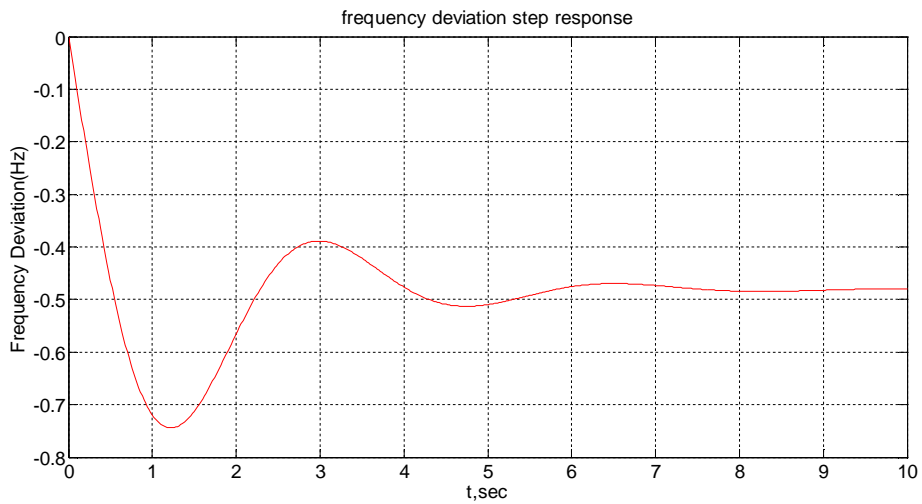


Figure 5.11: Frequency deviation step response (sudden load increase).

The speed-frequency relationship is related to the following equation

$$f = \frac{NP}{120}$$

Where, f = electrical frequency of generator, in Hz

P = number of poles in generator

N = speed of the prime mover, in rev/min

When the load of a generating station increases suddenly, the generators need to supply more power to load and so the speed of the prime mover drops causing a drop in frequency as well. But this drop of frequency is not allowed for maintaining the system stability. The change of frequency with the change of load is shown in Fig. 5.10 and Fig. 5.11. The code is given in Appendix D.7 and Appendix D.8.

This rise or drop of frequency is not allowed for maintaining the system stability. The sudden deviation of frequency should be recovered as soon as possible. This task is performed by the governor setting. The governor is capable of restoring the system frequency by increasing or decreasing the fuel supply if the frequency deviation is stable (sudden rising or falling). However, if the frequency deviation is not stable (oscillating in nature), then governor will fail. The unstable condition of frequency deviation is shown in Fig. 5.12. Appendix D.9 describes the Matlab code of Fig. 5.12.

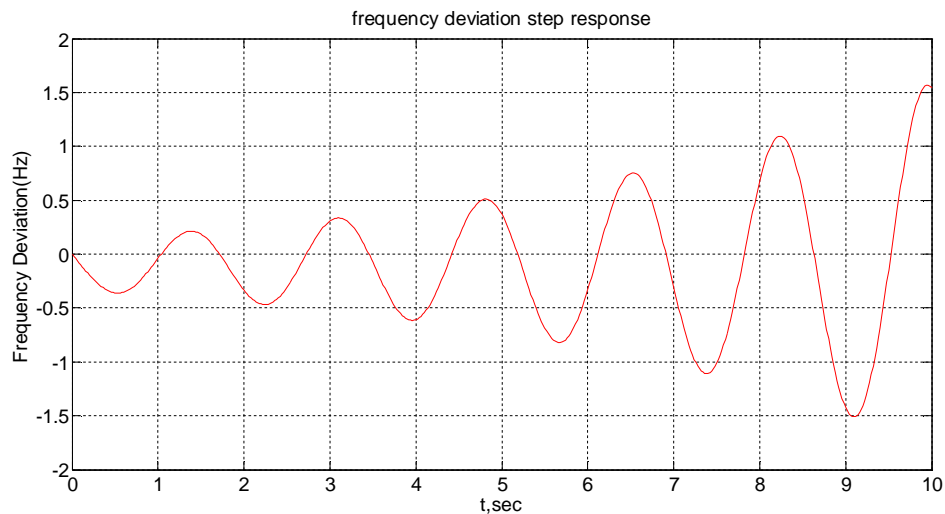


Figure 5.12: Unstable frequency deviation (after cyber-attack).

5.4.2 Proposed Solution

The frequency disturbance caused by cyber-attack may collapse the whole system stability. A solution is proposed in Fig. 5.13 to reduce the oscillating frequency deviation by connecting a

three input switch in the feedback path of LFC block.

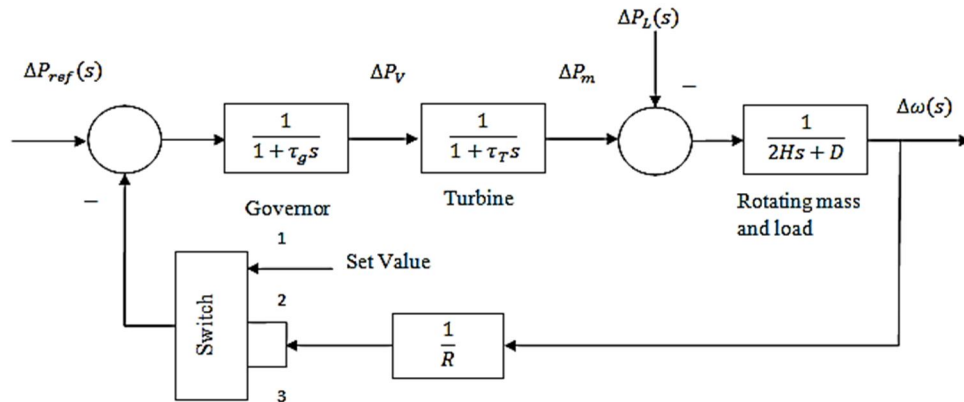


Figure 5.13: LFC with a three input switch.

The mathematical description of the switch is given below.

$$S.P = \begin{cases} U_1, & U_2 \geq \text{threshold} \\ U_3, & \text{else} \end{cases} \quad (5.3)$$

where, S.P = Switch passing terminal, U_1 = Input terminal 1, U_2 = Input terminal 2, U_3 = Input terminal 3.

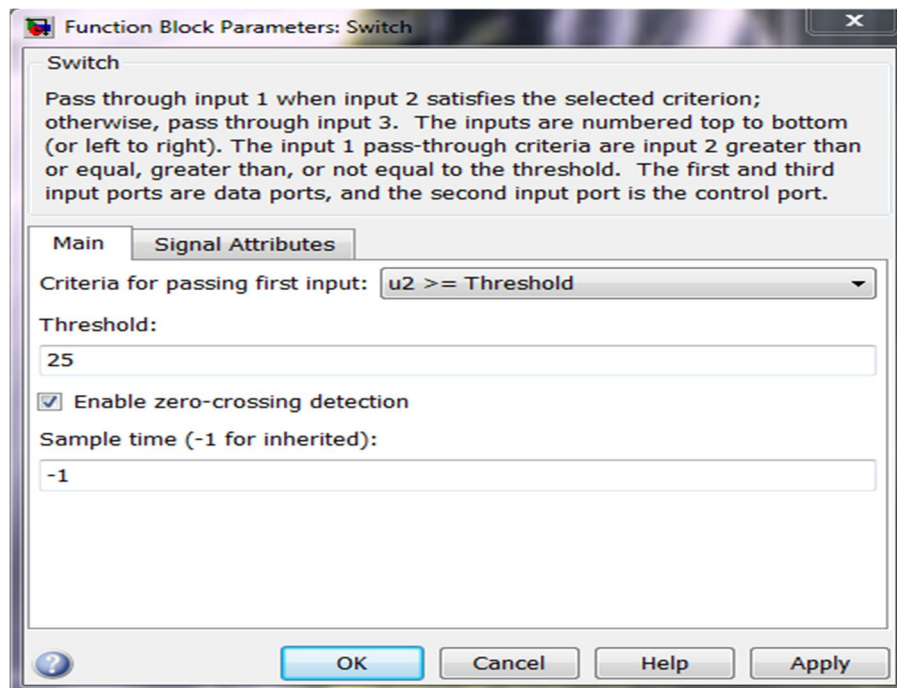


Figure 5.14: Switch properties [40].

The switch can mitigate the instability of frequency deviation caused by cyber-attack during sudden load change. The switch property is shown in Fig. 5.14.

From Fig. 5.4, it is seen that as the value of R decreasing from $0.05(1/R=1/.05=20)$, the frequency deviation is moving towards instability. That is why threshold value is chosen as $(1/R=1/.04) 25$, for injecting the set value after cyber-attack. The attack may be occurred due to unauthorized access to control system and also by injecting bad data to the system. When the value at input terminal 2 is greater than the threshold value that means R is less than 0.04 then the system tends to become unstable.

At this moment the switch activates the input terminal 1 to forcibly inject the set value to achieve system stability. When the input value at terminal 2 is less than the threshold, it seems that the system is stable and the switch allows input 3. Fig. 5.15 clearly represents the deviation of frequency during cyber attack before and after using the switch. Due to sudden load increase, the frequency deviates without any switch during the attack. Whereas, using the proposed switch the deviation of frequency can be minimized significantly.

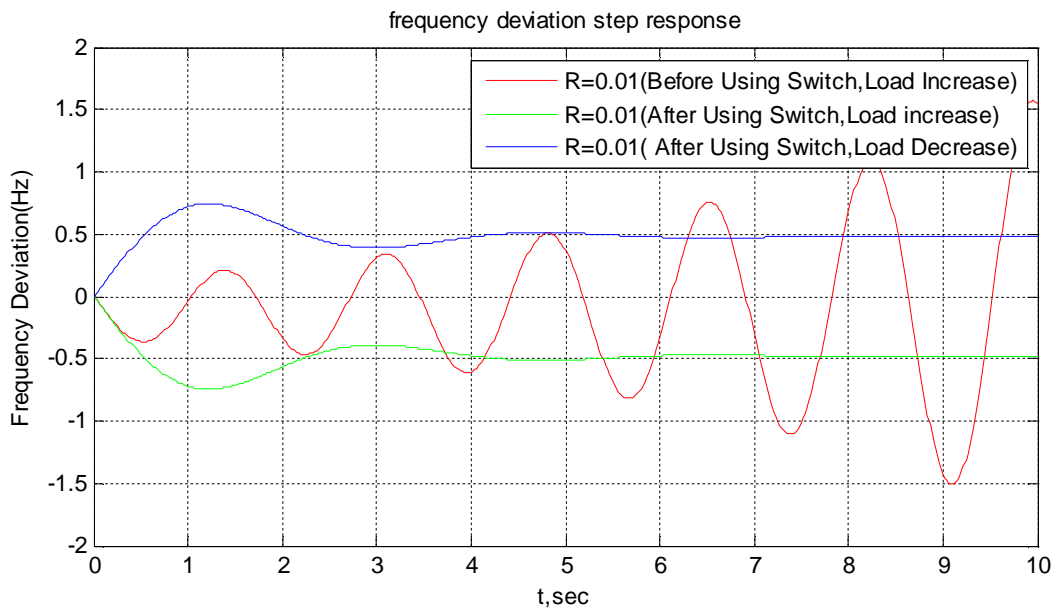


Figure 5.15: Frequency deviation before and after using the switch during cyber-attack (sudden load increase and decrease)

5.5 Summary

The frequency deviation and oscillation of power systems are shown as the impact of cyber-attack on an islanded power station during sudden changes of load in this chapter. Depending upon the nature of cyber-attack (positive biased attack or negative biased attack) simulation curves are developed and a solution method is proposed to make the system stable.

CHAPTER VI

Conclusion and Future Work

6.1 Contributions

To enhance the system stability and to reduce the possibility of voltage collapse, electrical test systems are analyzed through simulation process using PSAT (Power System Analysis Toolbox) in MATLAB. Different implementations of the control schemes utilizing proposed approach are examined and the most promising results are presented as follows:

- Voltage stability assessment of the WSCC 9-bus test system with STATCOM and SVC is investigated. The results show that a STATCOM provides higher voltage stability margin than a SVC.
- The reactive power support from the FACTS devices depends on the proper placement of the FACTS devices in the network. The power loss of the system is also improved if FACTS devices are used in the appropriate location. As the weakest bus requires highest reactive power, the proposed approach suggests placing the FACTS device at the weakest bus of the network. So, a STATCOM is installed at the weakest bus of the network that improves the power loss and static voltage stability of the system.
- Although a STATCOM improves the static voltage stability of the system, it is not always suitable for damping the oscillatory mode of the system. The small-signal stability assessment of IEEE 14-bus test system is conducted and a supplementary controller is designed using the real power deviation as input signal. The result shows that the proposed controller can enhance the damping performance of the system. It proves that a supplementary control law can be applied to existing devices to improve the dynamic performance of the system.
- The impact of cyber-attack is analyzed on LFC and AGC by considering their individual set value or stable limit parameter which can be a suitable means of cyber-attack. Positive biased attack on LFC causes the system frequency falls down but comes to stable condition quickly. Whereas it develops serious oscillation in frequency on AGC that makes the governor unable to set the appropriate point to restore system

frequency. For AGC, negative biased attack is not as serious as like positive one but frequency deviates highly with little oscillation in LFC.

- Proper connection of a three input switch in the feedback loop of LFC and appropriate assumption of its threshold value can efficiently mitigate the frequency disturbance of cyber hazard.

6.2 Future Work

Based on the work presented in this thesis, future research studies can be carried out in a number of aspects:

- Determining the optimum size of a STATCOM through static and dynamic analysis.
- To develop a robust damping controller for mitigating lightly-damped electro mechanical inter-area oscillations.
- Developing frameworks to identify cyber physical system vulnerabilities and determining the way of self- healing process to ensure cyber security of the control system against unauthorized access.

REFERENCES

- [1] “Global Trends in Renewable Energy Investment 2016”, published by Frankfurt School of Finance & Management, 2016.
- [2] P. Kundur, N. J. Balu, and M. G. Lauby, Power System Stability and Control, McGrawhill, 1994.
- [3] G. Rogers, Power System Oscillations, Kluwer Academic Publishers, 2000.
- [4] K. Prasertwong, N. Mithulanathan, and D. Thakur, "Understanding low-frequency oscillation in power systems," International Journal of Electrical Engineering Education, vol. 47, pp. 248-262, 2010.
- [5] Rahul Nema (M.E. Student), Dr. Anurag Trivedi (Associate Professor). “Load Frequency Control of a Small Isolated Power Station by Using Supercapacitor Based Energy Storage System,” International Journal of Advanced Research in Computer Engineering & Technology (IJARCET), vol. 1, pp. 162-167, December 2012.
- [6] Daniel E. Olivares, Ali Mehrizi-Sani, Amir H. Etemadi, Claudio A. Cañizares, Reza Iravani, Mehrdad Kazerani, Amir H. Hajimiragha, Oriol Gomis-Bellmunt, Maryam Saedifard, Rodrigo Palma-Behnke, Guillermo A. Jiménez-Estévez, and Nikos D. Hatziargyriou, “Trends in Microgrid Control,” IEEE Transactions on Smart Grid, Vol 5, pp. 1905 – 1919, July 2014
- [7] M.K. Jalboub, A.M. Ithal, H.S. Rajamtani, and R. A. Abd-Alhameed, “Determination of static voltage stability margin of the power system prior to voltage collapse,” 8th International Multi-Conference on Systems, Signals and Devices (SSD), pp. 1-6, March 2011.
- [8] Claudia Reis, F.P. Maciel Barbosa, “Indicators for voltage collapse margin,” Asia-Pacific Power and Energy Engineering Conference, pp. 1-4, 2010
- [9] A. Atputharajah, and T. K. Saha, “Power system blackouts - literature review,” International Conference on Industrial and Information Systems (ICIIS), pp. 460 – 465, 2009.
- [10] L. Baozhu and L. Bolong; “A novel static voltage stability index based on equilibrium solution region of branch power flow,” in Proc. IEEE Int. Conf. DRPT, China, pp. 809 – 814, Apr. 2008.
- [11] J. Zhao, Y. Wang, and P. Xu, “A comprehensive online voltage stability assessment

- method based on continuation power flow,” in Proc. IEEE Int. Conf. SUPERGEN, China, pp. 1-5 Apr. 2009.
- [12] C. Sharma and M. G. Ganness, “Determination of the applicability of using modal analysis for the prediction of voltage stability,” in Proc. IEEE Int. Conf. Trans. Distr., Chicago, pp. 1-7, Apr.2008.
- [13] Young-Hyun Moon et al., “Uniqueness of static voltage stability analysis in power systems,” in Power Engineering Society Summer Meeting, pp. 1536 – 1541, July 2001.
- [14] Li-Jun Cai, I. Erlich, “Power system static voltage stability analysis considering all active and reactive power controls - singular value approach,” in IEEE Power Tech, pp. 367 – 373, July 2007.
- [15] M. Mirzaei et al., “Static voltage stability analysis using generalized regression neural network,” IEEE 7th International Power Engineering and Optimization Conference (PEOCO), 3-4 June 2013.
- [16] F. A. Althowibi, M. W. Mustafa, “Maximum power systems loadability to detect voltage collapse,” 4th International Conference on Power Engineering and Optimization Conference (PEOCO), 23-24 June 2010.
- [17] S.D. Naik, M.K. Khedkar, S.S. Bhat, “On critical mode of bifurcation point and loadability in shunt compensated multi-bus power system,” in International Conference on Power and Energy Systems (ICPS), pp. 1- 6, 22-24 Dec. 2011.
- [18] J. Lakkireddy, “Steady state voltage stability enhancement using shunt and series FACTS devices,” in Clemson University Power Systems Conference (PSC), 10-13 March 2015.
- [19] P.C. Thomas, “Placement of STATCOM in a wind integrated power system with storage for improving the loadability of the system,” 7th International Conference on Intelligent Systems and Control (ISCO), pp. 31 – 35, 4-5 Jan. 2013.
- [20] J. Lakkireddy, “Steady state voltage stability enhancement using shunt and series FACTS devices,” Clemson University Power Systems Conference (PSC), 10-13 March 2015.
- [21] M.R.S. Tirtashi, A. Rohani, and R. Noroozian, "PSS and STATCOM controller design for damping power system oscillations using fuzzy control strategies," 18th Iranian Conference on Electrical Engineering (ICEE), pp.901-906, 11-13 May 2010.
- [22] H.S. Dalvi, and V.K. Chandrakar, "Voltage improvement using STATCOM for prototype hardware model, using synchronous and induction type generator," 3rd

International Conference on Emerging Trends in Engineering and Technology (ICETET), pp.413-417, 19-21 Nov. 2010.

- [23] S.P. Teeuwsen, "STATCOM with optimized POD controller for efficient inter-area oscillation damping," IEEE Power and Energy Society General Meeting (PES), pp.1-5, 21-25 July 2013.
- [24] S. Vishwakarma, R.K. Tripathi, "Transient energy dissipation and damping improvement using STATCOM & SSSC," International Conference on Power, Control and Embedded Systems (ICPCES), pp.1-4, Nov. 29 2010-Dec. 1 2010.
- [25] Bo Chen, Salman Mashayekh, Karen L. Butler-Purry, DeepaKundur, "Impact of Cyber Attacks on Transient Stability of Smart Grids with Voltage Support Devices," IEEE Power and Energy Society General Meeting (PES), pp.1-5, 2013.
- [26] Bo Chen, Karen L. Butler-Purry, DeepaKundur, "Impact Analysis of Transient stability Due to Cyber Attack on FACTS Devices," North American Power Symposium (NAPS), pp.1-6, 2013.
- [27] Yilin Mo, Tiffany Hyun-Jin Kim, Kenneth Brancik, Dona Dickinson, Heejo Lee, Adrian Perrig, Bruno Sinopoli, "Cyber-Physical Security of a Smart Grid Infrastructure," Proceedings of the IEEE, vol. 100, pp. 195 – 209, 2012.
- [28] Abdallah K. Farraj, Eman M. Hammad, Ashraf Al Daoud and DeepaKundur, "A Game-Theoretic Control Approach to Mitigate Cyber Switching Attacks in Smart Grid Systems," IEEE International Conference on Smart Grid Communications, pp. 958-963, 2014.
- [29] Mirjana Milosevic, Philippe Rosa, Marius Portmann, Goran Andersson, "Generation Control in Small Isolated Power Systems," IEEE Power and Energy Society General Meeting (PES), pp.1-8, 2007.
- [30] Abdallah Farraj, Eman M. Hammad, DeepaKundur, "On Using Distributed Control Schemes to Mitigate Switching Attacks in Smart Grids" IEEE 28th Canadian Conference on Electrical and Computer Engineering. Halifax, Canada, pp. 1578-1582, May 3-6, 2015.
- [31] Abdallah K. Farraj, Eman M. Hammad, Jin Wei, DeepaKundur, Karen L. Butler-Purry, "Performance of Flocking-Based Control Schemes in Smart Grid Applications," IEEE Global Conference on Signal and Information Processing for Energy Exchange and Intelligent Trading (GlobalSIP-14), pp. 233-237, 2014.
- [32] http://www.slideshare.net/jeevan_g/37426740-facts?related=1
- [33] http://www.gridtech.eu/project_scope/technologies/12-technologies/21-facts-flexible-alternating-current-transmission-system

- [34] Marakutulam D., editor, Proc. FACTS Conference I—The Future in High-Voltage Transmission, TR-100504, EPRI, March 1992.
- [35] N.G. Hingorani and L. Gyugyi, “Understanding FACTS: concepts and technology of flexible ac transmission systems”, IEEE Press, NY, 1999.
- [36] Baggini, A., Handbook of Power Quality, 2000.
- [37] F. Milano, “Power System Analysis Toolbox (PSAT) documentation,” Version 2.1.6.
- [38] L. Chun, J. Qirong, X. Xiaorong, and W. Zhonghong, “Rule-based control for STATCOM to increase power system stability,” in Power System Technology, Proceedings 1998 International Conference on POWERCON, Aug. 1998, pp. 372–376.
- [39] A. H. M. A. Rahim, S. A. Al-Baiyat, and H. M. Al-Maghrabi, “Robust damping controller design for a static compensator,” IEE Proceedings on Generation, Transmission and Distribution, vol. 149, pp. 491–496, July 2002.
- [40] M. H. Haque, “Improvement of first swing stability limit by utilizing full benefit of shunt FACTS devices,” IEEE Transactions on Power Systems, vol. 19, no. 4, pp. 1894–1902, 2004.
- [41] Brian Stott, “Review of Load-Flow Calculation Methods”, Proceedings of the IEEE , Vol. 62, No. 7, July 1974. pp 916-929.
- [42] E.Acha, C.R.Fuerte-Esquivel, H.Ambriz-perez, C.Angeles-Camacho, “FACTS Modelling and simulation in power networks,” John Willy & Sons, Ltd, 2004.
- [43] R. Mohan Mathur and Rajiv K. Varma, “Thyristor-Based FACTS Controllers for Electrical Transmission Systems,” IEEE Press, 2002.
- [44] W.D. Stevenson Jr., Elements of power system analysis, McGraw-Hill, 1982.
- [45] X. Duan, J. Chen, F. Peng, Y. Luo and Y. Huang, “Power Flow Control With FACTS Devices”, Power Engineering Society Summer Meeting, 2000. IEEE, Vol. 3, pp. 1585-1589.
- [46] E. Balagurusamy, Numerical methods, Tata Mc-Graw-Hill, New Delhi, 1999.
- [47] V. Ajjarapu and C. Christy, “The Continuation Power Flow: A Tool for Steady State Voltage Stability Analysis”, IEEE Transactions on Power Systems, Vol. 7, No. 1, February 1992, pp.416-423 .
- [48] A. R. Bergen, Power System Analysis, Prentice Hall, 2000.

- [49] R. Seydel, From Equilibrium to Chaos, Elsevier, 1988.
- [50] W. C. Rheinboldt and J. V. Burkardt, "A Locally Parameterized Continuation Process", ACM Transactions on Mathematical Software, Vol. 9, No. 2, June 1983, pp. 215-235.
- [51] D P Kothari, I J Nagrath, Modern power system Analysis, third edition, chapter -12, page- 304, 438.
- [52] HadiSaadat, Power System Analysis, Chapter – 12.
- [53] N.K. Roy, H.R. Pota and A. Anwar, "A new approach for wind and solar type DG placement in power distribution networks to enhance systems stability," IEEE Power Engineering and Optimization Conference (PEOCO), pp. 296-301, 6-7 June 2012.
- [54] R. Sadikovic, P. Korba, and G. Andersson, "Application of FACTS devices for damping of power system oscillations," IEEE Russia Power Tech, pp.1-6, 27-30 June 2005.
- [55] MATLAB 2010/Simulink Library Browser/Signal Routing/Switch.
- [56] S.K.M. Kodsı and C.A. Cañizares, "Modeling and simulation of IEEE 14 bus system with FACTS controllers," Technical report no. 2003-3, <https://ece.uwaterloo.ca/~ccanizar/papers/IEEEBenchmarkTFreport.pdf>.

Appendix A

Test system data of WSCC 9-bus test system is given in Table A.1.

Table A.1: Data of WSCC 9-bus system

Line no.	From bus - To bus	Resistance, R (pu)	Reactance, X (pu)	Susceptance, B (pu)
1	7 - 8	0.0085	0.072	0.149
2	6 - 9	0.039	0.170	0.358
3	5 - 7	0.032	0.161	0.306
4	4 - 5	0.01	0.085	0.176
5	4 - 6	0.017	0.092	0.158
6	8 - 9	0.0119	0.1008	0.209

Appendix B

The line and load data of IEEE 14-bus test system is given in Table B.1 and Table B.2 respectively [56].

Table B.1: Line data of IEEE 14-bus test system

From bus - To bus	Line charging (pu)	Tap ratio	Resistance, (pu)	Reactance, (pu)
1-2	0.0528	1	0.01938	0.05917
1-5	0.0492	1	0.05403	0.22304
2-3	0.0438	1	0.04699	0.19797
2-4	0.0374	1	0.05811	0.17632
2-5	0.034	1	0.05695	0.17388
3-4	0.0346	1	0.06701	0.17103
4-5	0.0128	1	0.01335	0.04211
4-7	0.00	0.978	0.00	0.20912
4-9	0.00	0.969	0.00	0.55618
5-6	0.00	0.932	0.00	0.25202
6-11	0.00	1	0.09498	0.1989
6-12	0.00	1	0.12291	0.25581
6-13	0.00	1	0.06615	0.13027
7-8	0.00	1	0.00	0.17615
7-9	0.00	1	0.00	0.11001
9-10	0.00	1	0.03181	0.08450
9-14	0.00	1	0.12711	0.27038
10-11	0.00	1	0.08205	0.19207
12-13	0.00	1	0.22092	0.19988
13-14	0.00	1	0.17093	0.34802

Table B.2: Load data of IEEE 14-bus test system

Bus no.	P_{load} (pu)	Q_{load} (pu)
1	0.00	0.00
2	0.2170	0.1270
3	0.9420	0.1900
4	0.4780	0.00
5	0.0760	0.0160
6	0.1120	0.0750
7	0.00	0.00
8	0.00	0.00
9	0.2950	0.1660
10	0.0900	0.0580
11	0.0350	0.0180
12	0.0610	0.0160
13	0.1350	0.0580
14	0.1490	0.0500

Appendix C

Synchronous generator at bus1: $f_n = 60$ Hz, $r_a = 0.001$ pu, $x_i = 0.2396$ pu, $x''_d = 0.23$ pu, $x'_d = 0.6$ pu, $x_d = 0.8979$ pu, $x''_q = 0.4$ pu, $x'_q = 0.646$ pu, $x_q = 0.646$ pu, $T'''_{do} = 0.03$ s, $T'_{do} = 7.4$ s, $T''_{qo} = 0$, $T'_{qo} = 0.033$ s, $M = 10.296$ s, $D = 2$ pu.

Excitation system: $K_a = 200$, $T_a = 0.02$ s, $V_{max} = 7.32$ pu, $V_{min} = 0$.

Synchronous generator at bus 2: $f_n = 60$ Hz, $r_a = 0.0031$ pu, $x_i = 0$, $x''_d = 0.13$ pu, $x'_d = 0.185$ pu, $x_d = 1.05$ pu; $x''_q = 0.13$ pu, $x'_q = 0.36$ pu, $x_q = 0.98$ pu, $T'''_{do} = 0.04$ s, $T'_{do} = 6.1$ s, $T''_{qo} = 0.099$ s, $T'_{qo} = 0.3$ s, $M = 13.08$ s, $D = 2$ pu.

Excitation system: $K_a = 20$, $T_a = 0.02$ s, $V_{max} = 4.38$ pu, $V_{min} = 0$.

Synchronous Condenser at bus3: $f_n = 60$ Hz, $r_a = 0.0031$ pu, $x_i = 0$, $x''_d = 0.13$ pu, $x'_d = 0.185$ pu, $x_d = 1.05$ pu; $x''_q = 0.13$ pu, $x'_q = 0.36$ pu, $x_q = 0.98$ pu, $T'''_{do} = 0.04$ s, $T'_{do} = 6.1$ s, $T''_{qo} = 0.099$ s, $T'_{qo} = 0.3$ s, $M = 13.08$ s, $D = 2$ pu.

Excitation system1: $K_a = 20$, $T_a = 0.02$ s, $V_{max} = 4.38$ pu, $V_{min} = 0$.

Synchronous Condenser at bus6: $f_n = 60$ Hz, $r_a = 0.0014$ pu, $x_i = 0.134$ pu, $x''_d = 0.12$ pu, $x'_d = 0.232$ pu, $x_d = 1.25$ pu; $x''_q = 0.12$ pu, $x'_q = 0.715$ pu, $x_q = 1.22$ pu, $T'''_{do} = 0.06$ s, $T'_{do} = 4.75$ s, $T''_{qo} = 0.21$ s, $T'_{qo} = 1.5$ s, $M = 10.12$ s, $D = 2$ pu.

Excitation system1: $K_a = 20$, $T_a = 0.02$ s, $V_{max} = 6.81$ pu, $V_{min} = 1.395$ pu.

Synchronous Condenser at bus8: $f_n = 60$ Hz, $r_a = 0.0014$ pu, $x_i = 0.134$ pu, $x''_d = 0.12$ pu, $x'_d = 0.232$ pu, $x_d = 1.25$ pu; $x''_q = 0.12$ pu, $x'_q = 0.715$ pu, $x_q = 1.22$ pu, $T'''_{do} = 0.06$ s, $T'_{do} = 4.75$ s, $T''_{qo} = 0.21$ s, $T'_{qo} = 1.5$ s, $M = 10.12$ s, $D = 2$ pu.

Excitation system1: $K_a = 20$, $T_a = 0.02$ s, $V_{max} = 6.81$ pu, $V_{min} = 1.395$ pu.

STATCOM parameters: $K_r = 50$, $T_r = 0.1$ s, $i_{max} = 0.2$ pu, $i_{min} = -0.2$ pu

Appendix D

D.1 Source code of frequency deviation step response for different values of governor speed regulation

```

pl=0.2;
t=0:.02:10;
num1=[0.1 0.7 1];
dnum1=[1 7.08 10.56 20.8];
dnum2=[1 7.08 10.56 50.8];
dnum3=[1 7.08 10.56 74.87];
dnum4=[1 7.08 10.56 103.89];
Freq1= -pl*50*step(num1,dnum1,t);
Freq2= -pl*50*step(num1,dnum2,t);
Freq3= -pl*50*step(num1,dnum3,t);
Freq4= -pl*50*step(num1,dnum4,t);
plot(t,Freq1,'r');hold on;
plot(t,Freq2,'y');
plot(t,Freq3,'b');
plot(t,Freq4,'g');hold off;
legend('R=0.05','R=0.02','R=0.0135','R=0.0097');
xlabel('t,sec')
ylabel('Frequency Deviation(Hz)')
title('frequency deviation step response')
grid on

```

D.2 Source code for determining frequency deviation step response for LFC under positively biased attack condition

```

pl=0.2;
t=0:.02:10;
R= 20.8;
num1=[0.1 0.7 1];
dnum1=[1 7.08 10.56 R];
dnum2=[1 7.08 10.56 17.47];
dnum3=[1 7.08 10.56 15.09];
dnum4=[1 7.08 10.56 13.3];
Freq1= -pl*50*step(num1,dnum1,t);
Freq2= -pl*50*step(num1,dnum2,t);
Freq3= -pl*50*step(num1,dnum3,t);

```

```

Freq4= -pl*50*step(num1,dnum4,t);
plot(t,Freq1,'r');hold on;
plot(t,Freq2,'y');
plot(t,Freq3,'b');
plot(t,Freq4,'g');hold off;
legend('R=0.05','R=0.06','R=0.07','R=0.08');
xlabel('t,sec')
ylabel('Frequency Deviation(Hz)')
title('frequency deviation step response')
grid on

```

D.3 Source code for determining frequency deviation step response for LFC under negatively biased attack condition

```

pl=0.2;
t=0:.02:10;
num1=[0.1 0.7 1];
dnum1=[1 7.08 10.56 20.8];
dnum2=[1 7.08 10.56 34.13];
dnum3=[1 7.08 10.56 100.8];
dnum4=[1 7.08 10.56 111.91];
Freq1= -pl*50*step(num1,dnum1,t);
Freq2= -pl*50*step(num1,dnum2,t);
Freq3= -pl*50*step(num1,dnum3,t);
Freq4= -pl*50*step(num1,dnum4,t);
plot(t,Freq1,'r');hold on;
plot(t,Freq2,'y');
plot(t,Freq3,'b');
plot(t,Freq4,'g');hold off;
legend('R=0.05','R=0.03','R=0.01','R=0.009');
xlabel('t,sec')
ylabel('Frequency Deviation(Hz)')
title('frequency deviation step response')
grid on

```

D.4 Source code for determining frequency deviation step response for AGC

```

pl=0.2;
t=0:.02:12;
k1=4;
k2=7;
k3=10;
k4=15;

```

```

num=[0.1 0.7 1 0];
dnum1=[1 7.08 10.56 20.8 ki1];
dnum2=[1 7.08 10.56 20.8 ki2];
dnum3=[1 7.08 10.56 20.8 ki3];
dnum4=[1 7.08 10.56 20.8 ki4];
c1=-pl*50*step(num,dnum1,t);
c2=-pl*50*step(num,dnum2,t);
c3=-pl*50*step(num,dnum3,t);
c4=-pl*50*step(num,dnum4,t);
plot(t,c1,'r');hold on;
plot(t,c2,'y');
plot(t,c3,'b');
plot(t,c4,'g');hold off;
legend('ki=4','ki=7','ki=10','ki=15');
xlabel('t,sec')
ylabel('Frequency Deviation(Hz)')
title('frequency deviation step response')
grid on

```

D.5 Source code for determining frequency deviation step response for AGC under positively biased attack condition

```

pl=0.2;
t=0:.02:12;
ki1=7;
ki2=9;
ki3=10;
ki4=15;
num=[0.1 0.7 1 0];
dnum1=[1 7.08 10.56 20.8 ki1];
dnum2=[1 7.08 10.56 20.8 ki2];
dnum3=[1 7.08 10.56 20.8 ki3];
dnum4=[1 7.08 10.56 20.8 ki4];
c1=-pl*50*step(num,dnum1,t);
c2=-pl*50*step(num,dnum2,t);
c3=-pl*50*step(num,dnum3,t);
c4=-pl*50*step(num,dnum4,t);
plot(t,c1,'r');hold on;
plot(t,c2,'y');
plot(t,c3,'b');
plot(t,c4,'g');hold off;
legend('ki=7','ki=9','ki=10','ki=15');
xlabel('t,sec');

```

```

ylabel('Frequency Deviation(Hz)');
title('Frequency Deviation Step Response');
grid on

```

D.6 Source code for determining frequency deviation step response for AGC under negatively biased attack condition

```

pl=0.2;
t=0:.02:12;
ki1=7;
ki2=4;
ki3=3;
ki4=2;
num=[0.1 0.7 1 0];
dnum1=[1 7.08 10.56 20.8 ki1];
dnum2=[1 7.08 10.56 20.8 ki2];
dnum3=[1 7.08 10.56 20.8 ki3];
dnum4=[1 7.08 10.56 20.8 ki4];
c1=-pl*50*step(num,dnum1,t);
c2=-pl*50*step(num,dnum2,t);
c3=-pl*50*step(num,dnum3,t);
c4=-pl*50*step(num,dnum4,t);
plot(t,c1,'r');hold on;
plot(t,c2,'y');
plot(t,c3,'b');
plot(t,c4,'g');hold off;
legend('ki=7','ki=4','ki=3','ki=2');
xlabel('t,sec');
ylabel('Frequency Deviation(Hz)');
title('Frequency Deviation Step Response');
grid on

```

D.7 Source code for determining frequency deviation step response under sudden load decrease

```

pl=0.2;
t=0:.02:10;
num1=[0.1 0.7 1];
dnum1=[1 7.08 10.56 20.8];
Freq1= pl*50*step(num1,dnum1,t);
plot(t,Freq1,'r');
xlabel('t,sec')
ylabel('Frequency Deviation(Hz)')

```

```
title('frequency deviation step response')
grid on
```

D.8 Source code for determining frequency deviation step response under sudden load increase

```
p1=0.2;
t=0:.02:10;
num1=[0.1 0.7 1];
dnum1=[1 7.08 10.56 20.8];
Freq1= -p1*50*step(num1,dnum1,t);
plot(t,Freq1,'r');
xlabel('t,sec')
ylabel('Frequency Deviation(Hz)')
title('frequency deviation step response')
grid on
```

D.9 Source code for determining frequency deviation step response using switch in LFC loop under sudden load change

```
p1=0.2;
t=0:.02:10;
num1=[0.1 0.7 1];
dnum1=[1 7.08 10.56 20.8];
dnum2=[1 7.08 10.56 100.8];
Freq1= -p1*50*step(num1,dnum2,t);
Freq2= -p1*50*step(num1,dnum1,t);
Freq3= p1*50*step(num1,dnum1,t);
plot(t,Freq1,'r'); hold on
plot(t,Freq2,'g');
plot(t,Freq3,'b');hold off
legend('R=0.01(Before Using Switch,Load Increase)', 'R=0.01(After Using Switch,Load increase)', 'R=0.01( After Using Switch,Load Decrease)');
xlabel('t,sec')
ylabel('Frequency Deviation(Hz)')
title('frequency deviation step response')
grid on
```

LIST OF PUBLICATIONS

- [1] **Mehedi Hassan**, N. K. Roy, and Md. Sahabuddin, “ Mitigation of Frequency Disturbance in Power Systems during Cyber-Attack,” IEEE co-sponsored International Conference on Electrical, Computer & Telecommunication Engineering (ICECTE), 2016.
- [2] **Mehedi Hassan**, Kazi Md. Shahiduzzaman and N.K. Roy, “Static Voltage Stability Assessment of Power Systems with FACTS Devices,” IOSR Journal of Electrical and Electronics Engineering (IOSR-JEEE), vol. 11, issue 2, ver. I, pp. 38-41, Mar. – Apr. 2016.
- [3] **Mehedi Hassan** and N. K. Roy, “Damping of Power System Oscillations using STATCOM,” IEEE Conference on Electrical Information and Communication Technology (EICT), pp. 545-548, 10-12 Dec. 2015.